MINIMUM ORBITS ABOUT THE PLANET VENUS

THESIS

Jeffrey J. Smith
Captain, USAF

AFIT/GA/ENY/90D-12

DEPARTMENT OF THE AIR FORCE
AIR UNIVERSITY
AIR FORCE INSTITUTE OF TECHNOLOGY

Wright-Patterson Air Force Base, Ohio

AFIT/GA/ENY/90D-12

MINIMUM ORBITS ABOUT THE PLANET VENUS

THESIS

Jeffrey J. Smith
Captain, USAF

AFIT/GA/ENY/90D-12

AFIT/GA/ENY/90D-12

MINIMUM ORBITS ABOUT THE PLANET VENUS

THESIS

Presented to the Faculty of the School of Engineering

of the Air Force Institute of Technology

Air University

In Partial Fulfillment of the

Requirements for the Degree of

Master of Science in Astronautical Engineering

Jeffrey J. Smith, B.S.

Captain, USAF

November 1990

Acknowledgements

I would like to express my thanks to my advisor, Capt Bain, for his guidance; to Steve, Bob, and Ken for helping me get to this point; to Jeff, for providing some much-needed perspective towards the end (and the use of his computer just in the nick of time); and especially to my wife Sherrill, for tolerating all of this.

J. J. Smith

Table of Contents

List of Figures

List of Tables

Notation

A	satellite frontal area
AU	Astronomical Unit
$\mathbf{a}$	acceleration vector
$\mathbf{a}_g$	acceleration due to gravity
$\mathbf{a}_d$	acceleration due to drag
$\mathbf{a}_{srp}$	acceleration due to solar radiation pressure
$\mathbf{a}_{tb}$	acceleration due to third body
a	semi-major axis
β	ballistic coefficient or inverse of scale height
C_D	coefficient of drag
C_{nk}	gravity field constant
E	eccentric anomaly
e	eccentricity
ϵ	planetary ellipticity
G	universal gravitational constant
γ	reflectivity factor
H	scale height
h	altitude
h_g	ellipsoidal altitude
i	inclination
J_n	zonal gravitational coefficient
Λ	geometric mean longitude of the sun
M	mass of the primary
M_w	molecular weight of the atmosphere
m	mass of the satellite
μ	product of G and M
n	mean motion
ν	true anomaly
Ω	longitude of ascending node
ω	argument of periapsis
ω_a	rotation rate of the atmosphere

P_R	solar radiation pressue at 1 *AU*
P	pressure
P_n^k	Legendre Polynomial
P_n	Associated Legendre Polynomial
Φ	longitude
Ψ	planetary density function
R_e	planetary equatorial radius
R^*	universal gas constant
$\mathbf{r}$	position vector
r	radius
r_{occ}	occultation radius
$\vec{\rho}$	relative position vector
ρ	atmospheric density
S_{nk}	gravity field constant
T	temperature
θ	co-latitude
U	geopotential function
$\mathbf{v}$	velocity vector
v	velocity
v_a	atmospheric velocity
x, y, z	rectangular coordinates
ζ	obliquity of the ecliptic

Abstract

An investigation is conducted into low orbiting satellites about the planet Venus with drag limited lifetimes. It is possible to specify combinations of orbital elements which result in orbital lifetimes greater than some desired value. These combinations can be assembled into Critical Curves and Critical Surfaces. Critical Curves and Critical Surfaces are defined as the curve or surface in orbital element space above which initial element sets will result in orbits that meet or exceed lifetime requirements

A numerical method is implemented for finding these combinations, and three Critical Surfaces are examined. A "decay threshold" is selected for bounding satellite lifetime. Numerical simulations of orbital behavior are conducted, and polynomials describing the Critical Curves are produced for five different eccentricities at each of three decay thresholds. Comparisons of the effects of the different perturbations considered (geopotential, atmospheric drag, third body effects, and solar radiation pressure) and of decay threshold altitude variations are made.

MINIMUM ORBITS ABOUT THE PLANET VENUS

I. Introduction

Background

Orbital elements are initially determined to meet specific mission objectives. These objectives may be in terms of ground track coverage, communications coverage, or other criteria. For example, Cain [3] has determined element sets which will result in orbits containing arcs of minimum altitude variation. These orbits would be useful for missions utilizing sensors which are extremely sensitive to altitude variations, but are also extremely susceptible to decay due to drag, because of low altitudes and eccentricities. All orbital elements will tend to stray from their nominal values. These perturbations are caused by various forces acting on the satellite, and can result in orbital decay to the extent that the satellite reenters the atmosphere. Satellite lifetime is therefore an important concern to mission planners.

It is possible to determine combinations of orbital elements which specify an orbit which meets a given criteria for orbit lifetime. This could be described as a minimum or critical orbit. If these critical element sets are known over a wide range of element values, a "Critical Surface" may be constructed (in six dimensional element space), above which satellite lifetime can be guaranteed to meet or exceed the lifetime criteria. This Critical Surface may then be used as an aid in determining initial element sets which would fulfill other requirements and meet

a minimum lifetime specification. This would be particularly useful for low altitude lightsats with limited or no station-keeping capabilities.

Drag is the predominant perturbation involved in the decay of low altitude satellites. In determining these minimum orbits, drag therefore must be taken into account. To accurately model the satellite lifetime, other significant perturbations must also be included. A decay threshold must be selected below which the satellite is considered to have "reentered" in order to definitively bound lifetime. In order to produce the Critical Surface, a wide range of initial elements is required, but orbits where drag is not the most influential perturbation are not considered. In these cases, the orbital elements will be perturbed from the nominal values, but the perturbations will not necessarily result in orbital decay. Drag is most predominant for orbits with low eccentricities, so only orbits with fairly low eccentricities will be addressed.

Objective

A method of determining the Critical Surface was derived (see Chapter III, *Search Method*). Three Critical Surfaces for the planet Venus, based on three slightly different decay thresholds, were specified by this method. Geopotential effects, atmospheric drag, solar third body effects, and solar radiation pressure were considered.

Approach

A search method was employed to determine the minimum semi-major axis for a given eccentricity and inclination such that the orbit did not

decay to the point of reentry before 90 earth days had elapsed. If an axisymmetric planet is considered, the longitude of ascending node, argument of periapsis and true anomaly may be set to any arbitrary value without changing the effect of the perturbations considered, and the convenient value of zero was used. This limited the effective orbital element space to three dimensions. The method was employed over a range of eccentricities and inclinations. Polynomials were then fitted to these initial element sets to obtain equations describing general relationships between the elements in question. Three Critical Surfaces were generated in this fashion.

II. Analytical Model

Satellite Motion

A satellite affected only by the gravitational attraction of a spherical, homogeneous planet would exhibit "two-body," or Keplerian, motion. The two-body solution positions the satellite by means of six variables (semi-major axis a, eccentricity e, inclination i, longitude of ascending node Ω, argument of periapsis ω, and true anomaly ν). With the exception of the true anomaly, which locates the satellite along the orbit, these would not change with time. The satellite would continue to follow the same orbit indefinitely. In reality, a host of lesser forces act on the satellite, "perturbing" the orbit and causing the orbital elements to change over time. In order to study the effects of the perturbations it is necessary to model both the ideal two-body motion and the perturbations of interest.

Perturbations may give rise to periodic effects, secular effects, or both. Periodic effects result in no net change in the orbital elements, but vary the elements around some nominal value. Secular effects do change the elements with time, and are of primary interest here. The effect a given perturbation may have on a specific orbital element is not necessarily in proportion to its magnitude.

The position and velocity of a satellite may be found from:

$$\mathbf{f} = \mathbf{a} \tag{1}$$

where $\ddot{\mathbf{r}}$ is the inertial acceleration of the satellite and $\mathbf{a}$ is the sum of the accelerations caused by perturbative forces acting on the satellite. This chapter will present the relationships and equations used to model two-body motion and perturbative accelerations due to the geopotential, air drag, third body effects and solar radiation pressure. These accelerations produce perturbations which can be averaged over the orbital period to give the net change in each element over one period, and these averaged equations are also presented.

Gravitational Attraction

Two-Body Motion. The two-body motion contribution to **a** in Equation (1) is the acceleration due to the gravity of the primary, modeled as a point mass. Gravity obeys an "inverse square" law, with gravitational attraction falling off as the inverse of the distance squared. This can be written as:

$$\ddot{\mathbf{r}} = -\mu \frac{\mathbf{r}}{r^3} \tag{2}$$

where **r** is the position of the satellite and μ is the product of the mass of the planet (M) and the universal gravitational constant (G). This can be shown to result in motion according to the equation describing a conic, or Kepler's Equation:

$$r = \frac{a(1-e^2)}{1+e\cos(\nu)} \tag{3}$$

where r is the distance from the center of the planet to the satellite [2: 20].

Geopotential. The potential function that results in the right side of equation (2) is $V = -\mu/r$. Taking the gradient of this scalar function results in the vector acceleration **a** referenced in Equation (1):

$$\mathbf{a} = \nabla V \tag{4}$$

Newton showed that this potential can be extended to a planet that could be modeled as a series of concentric homogeneous spherical shells. Unfortunately, real planets deviate greatly from this model, severely limiting its accuracy.

At this point it is necessary to develop a geopotential function that

will allow a non-spherical, non-homogeneous planet. To do this, Equation (4) is used considering V as an unknown. With **a** given by the acceleration due to a point mass, as in Equation (2), Equation (4) is integrated over the surface of a unit sphere. This results in Poisson's Equation for gravitational fields:

$$\nabla^2 V = -4\pi G\psi \tag{5}$$

from which any V may be found as a function of position, given $\psi(x,y,z)$ -- the density distribution of the central body. Considering only those orbits outside the planetary surface (where $\psi(x,y,z)=0$) reduces Equation (5) to Laplace's Equation:

$$\nabla^2 V = 0 \tag{6}$$

Since the bodies of interest are nearly spherical, Equation (6) is expressed in spherical coordinates:

$$\nabla^2 V = \frac{1}{r^2}\frac{\partial}{\partial r}\left(r^2\frac{\partial V}{\partial r}\right) + \frac{1}{r^2\sin\theta}\frac{\partial}{\partial\theta}\left(\sin\theta\frac{\partial V}{\partial\theta}\right) + \frac{1}{r^2\sin^2\theta}\frac{\partial^2 V}{\partial\phi^2} = 0 \tag{7}$$

where r is the radius to the point of interest, θ is the co-latitude, and ϕ is the longitude. This is a linear partial differential equation, and can be separated into three functions of r, θ, and ϕ respectively. The separated function of ϕ describes a simple harmonic oscillator. Considered with the appropriate boundary conditions, its solution becomes:

$$F(\phi) = C_k\cos k\phi + S_k\sin k\phi \tag{8}$$

Separating the function of θ results in:

$$\frac{1}{\sin\theta}\frac{d}{d\theta}\left(\sin\theta\frac{dF(\theta)}{d\theta}\right) - \left(\frac{m^2}{\sin^2\theta} - l\right)F(\theta) = 0 \tag{9}$$

which is recognizable as Legendre's Equation, and is solved by the Associated Legendre Polynomials:

$$F(\theta) = P_n^k(\cos\theta) \tag{10}$$

Lastly, the function of r yields two solutions, only one of which is physically meaningful. This leaves:

$$F(r) = r^{-n-1} = \left(\frac{r}{R_\bullet}\right) \tag{11}$$

where $R_\bullet$ is the planetary equatorial radius. Equations (8), (10) and (11) are combined to produce an infinite series solution to Equation (7):

$$V(r,\theta,\phi) = -\frac{\mu}{r}\sum_{n=0}^{\infty}\sum_{k=0}^{n}\left(\frac{r}{R_\bullet}\right)^{-n} P_n^k(\cos\theta)(C_{nk}\cos k\phi + S_{nk}\sin k\phi) \tag{12}$$

C_{nk} and S_{nk} are now constants defining the shape of the gravitational field [7: 7]. The lead-off term in this series will be the point mass potential term. This function, with C_{nk} and S_{nk} supplied by an appropriate gravity model for the planet in question, defines the gravitational field the satellite operates in and may be employed to determine the acceleration on the satellite due to the geopotential:

$$\mathbf{a}_g = \nabla V \tag{13}$$

Gravity models for most of the explored planets have been compiled from empirical data [15].

If the primary of interest can be modeled as an axisymmetric planet (a planet of the form of a solid of rotation about the polar axis, where the ellipticity describes the "out of roundness" of a meridian, but parallels of latitude are perfect circles) then Equation (12) can be simplified. In this case, there is no dependence on the variable ϕ and the index k

is fixed at zero. The $S_{nk}\sin k\phi$ term goes to zero, and the $C_{nk}\cos k\phi$ term becomes C_{n0}. The Associated Legendre Polynomial P_n^0 is equivalent to the Legendre Polynomial P_n. With the replacement of C_{n0} with $-J_n$, Equation (12) reduces to:

$$V = \left(\frac{\mu}{r}\right)\left[1 - \sum_{n=2}^{\infty} J_n\left(\frac{R_\bullet}{r}\right)^n P_n(\cos\theta)\right] \qquad (14)$$

which is the geopotential expansion for an axisymmetric planet. The terms resulting from this series are called "zonal harmonics." This model will be concerned with this expansion through the sixth order zonal harmonics. The coefficients (J_2, J_3, etc.) used in computing the zonal harmonics for Venus are given in Appendix A, Table A-1.

Averaged Equations for Geopotential. Merson [11] produced averaged equations for the change in each of the elements due to geopotential expansion terms for $J_2 - J_6$ over one orbital period, and his results are presented here. If the inclination or the eccentricity is zero, the equation for the change in argument of periapsis is not valid, and if the inclination is zero the equation for longitude of ascending node is not valid. Merson also included terms for the change in the elements due to $(J_2)^2$, since for earth $(J_2)^2$ is of the same order of magnitude as $J_3 - J_6$. This is not the case with Venus, where the J_2 term is not nearly as predominant as with the earth (see Table 1). Therefore, the $(J_2)^2$ terms have been culled from the equations presented here.

The change in the semi-major axis is entirely dependent on the

$(J_2)^2$ term and is therefore negligible. The change in the other elements is given by:

$$\Delta x = 2\pi\left[\sum_{n=0}^{6} J_n\left(\frac{R_\bullet}{a(1-e^2)}\right)^n x_n\right] \qquad (15)$$

where Δx is replaced with Δe, Δi, $\Delta\Omega$ or $\Delta\omega$, and x_n is replaced by the appropriate term from the equations below.

$$e_2 = 0$$

$$e_3 = -3/2(1-e^2)\sin i\cos\omega(1-5/4\sin^2 i)$$

$$e_4 = -45/16(1-e^2)(1-7/6\sin^2 i)e\sin^2 i\sin 2\omega$$

$$e_5 = 15/4(1-e^2)\sin i\Big[(1-7/2\sin^2 i+21/8\sin^4 i)(1+3/4e^2)\cos\omega$$
$$+7/8(1-9/8\sin^2 i)e^2\sin^2 i\cos 3\omega\Big]$$

$$e_6 = 525/32(1-e^2)\sin^2 i\Big[(1-3\sin^2 i+33/16\sin^4 i)(1+1/2e^2)e\sin 2\omega$$
$$+3/16(1-11/10\sin^2 i)e^3\sin^2 i\sin 4\omega\Big]$$

$$i_2 = 0$$

$$i_3 = 3/2(1-5/4\sin^2 i)e\cos\omega\cos i$$

$$i_4 = 45/32(1-7/6\sin^2 i)e^2\sin 2\omega\sin 2i$$

$$i_5 = -15/4e\cos i\Big[(1-7/2\sin^2 i+21/8\sin^4 i)(1+3/4e^2)\cos\omega$$
$$+7/8(1-9/8\sin^2 i)e^2\sin^2 i\cos 3\omega\Big]$$

$$i_6 = -525/64 e \sin 2i \Big[(1 - 3\sin^2 i + 33/16 \sin^4 i)(1 + 1/2 e^2) e \sin 2\omega$$

$$+ 3/16 (1 - 11/10 \sin^2 i) e^3 \sin^2 i \sin 4\omega \Big]$$

$$\Omega_2 = -3/2 \cos i$$

$$\Omega_3 = 3/2 (1 - 15/4 \sin^2 i) e \sin\omega \cot i$$

$$\Omega_4 = 15/4 \cos i [(1 - 7/4 \sin^2 i)(1 + 3/2 e^2) - 3/4 (1 - 7/3 \sin^2 i) e^2 \cos 2\omega]$$

$$\Omega_5 = -15/4 \cot i \Big[(1 - 21/2 \sin^2 i + 105/8 \sin^4 i)(1 + 3/4 e^2) e \sin\omega$$

$$+ 7/8 (1 - 15/8 \sin^2 i) e^3 \sin 3\omega \Big]$$

$$\Omega_6 = -105/16 \cos i \Big[(1 - 9/2 \sin^2 i + 33/8 \sin^4 i)(1 + 5e^2 + 15/8 e^4)$$

$$- 5/2 (1 - 6\sin^2 i + 99/16 \sin^4 i)(1 + 1/2 e^2) e^2 \cos 2\omega$$

$$- 15/32 (1 - 33/20 \sin^2 i) e^4 \sin^2 i \cos 4\omega \Big]$$

$$\omega_2 = 3(1 - 5/4 \sin^2 i)$$

$$\omega_3 = 3/2 e^{-1} \sin\omega \sin i [(1 - 5/4 \sin^2 i) + (35/4 \cos^2 i - \operatorname{cosec}^2 i) e^2]$$

$$\omega_4 = -15/32 \Big[(16 - 62 \sin^2 i + 49 \sin^4 i) + (6 \sin^2 i - 7 \sin^2 i) \cos 2\omega + \Big(18$$

$$- 63 \sin^2 i + 189/4 \sin^4 i \Big) e^2 + (-6 + 35 \sin^2 i - 63/2 \sin^4 i) e^2 \cos 2\omega \Big]$$

$$\omega_5 = 105/16 e^{-1} \sin\omega \operatorname{cosec} i \Big[(-4/7 + 2\sin^2 i - 3/2 \sin^4 i) \sin^2 i + \Big(4/7$$

$$- 87/7 \sin^2 i + 67/2 \sin^4 i - 357/16 \sin^6 i \Big) e^2 + (-1 + 9/8 \sin^2 i)$$

$$e^2 \sin^4 i \cos 2\omega + (3/7 - 7\sin^2 i + 267/16 \sin^4 i - 165/16 \sin^6 i) e^4$$

$$+ (1 - 39/8 \sin^2 i + 33/8 \sin^4 i) e^4 \sin^2 i \cos 2\omega \Big]$$

$$\omega_6 = 525/64\Big[8/5(1-8\sin^2 i\,129/8\sin^4 i-297/32\sin^6 i)+\Big(2-6\sin^2 i$$

$$+33/8\sin^4 i\Big)\sin^2 i\cos 2\omega+6\Big(1-43/6\sin^2 i+109/8\sin^4 i-121/8$$

$$\sin^6 i\Big)e^2+(-2+25\sin^2 i-459/8\sin^4 i+561/16\sin^6 i)e^2\cos 2\omega$$

$$+3/8(1-11/10\sin^2 i)e^2\sin^4 i\cos 4\omega+\Big(2-27/2\sin^2 i+99/4\sin^4 i$$

$$-429/32\sin^6 i\Big)e^4+(-1+21/2\sin^2 i-363/16\sin^4 i+429/32\sin^6 i)$$

$$e^4\cos 2\omega+3/8(-1+22/5\sin^2 i-143/40\sin^4 i)e^4\sin^2 i\cos 4\omega\Big]$$

These equations may be used to determine the secular changes to the orbital elements due to geopotential which occur in one orbit -- periodic perturbations with a period of less than one orbital period are averaged out.

Atmospheric Perturbations

Air Drag. The motion of a satellite through the upper atmosphere of a planet subjects the satellite to aerodynamic forces which can perturb the orbit. Atmospheric forces cause an acceleration in the direction opposite the velocity with respect to the atmosphere (commonly called drag), and an acceleration perpendicular to the velocity vector. The perpendicular component does not necessarily pass through the satellite's center of mass, resulting in both a "lift" force and a "lift" moment about the center of mass. Figure 1 illustrates the aerodynamic forces on a satellite.

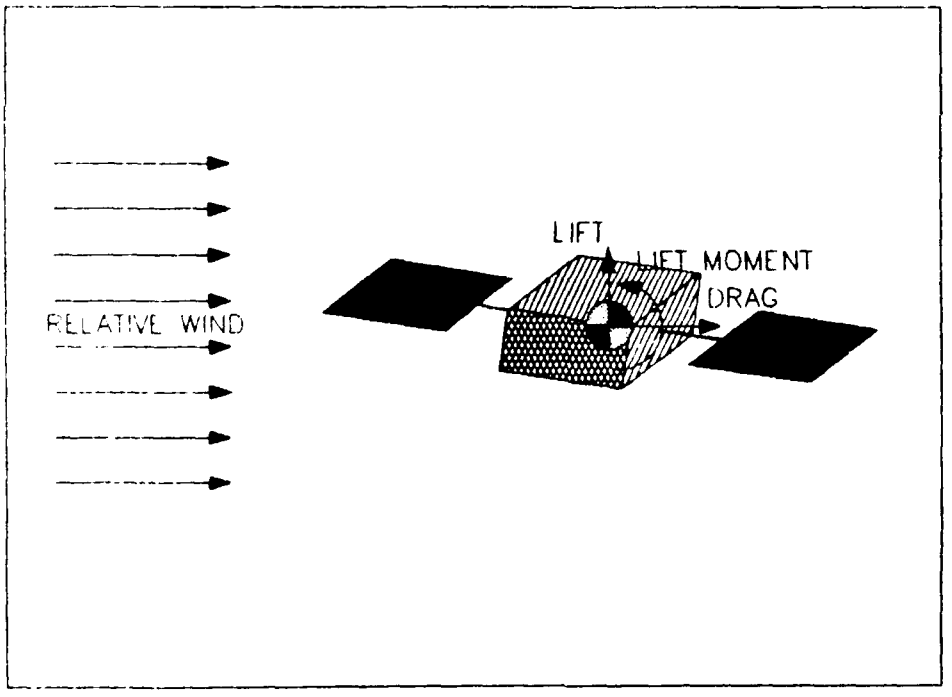

Figure 1. Atmospheric Forces on the Satellite

The direction of the perpendicular component at any time is a function of satellite attitude. It is reasonable to assume that the perpendicular component is small compared to the other component, and that the design and attitude of the satellite over time will drive the resultant acceleration towards zero, so that this component can be ignored [8: 13]. The acceleration due to drag is then given by:

$$a_d \approx -\frac{C_D A}{2m}\rho v v \tag{16}$$

where C_D is the coefficient of drag for the satellite, A is the frontal area the satellite presents to the airstream, m is the satellite mass, ρ is the atmospheric density, and v is the velocity with respect to the atmosphere. To simplify parametric analysis, a "ballistic coefficient" β is often introduced where $\beta = \frac{C_D A}{2m}$. Each of these factors will now be examined in turn.

Ballistic Coefficient. Starting with the simplest term of the ballistic coefficient, the mass of the satellite may be either fixed or a function of time. The mass obviously has an affect on the acceleration that drag will produce on the satellite (a less massive satellite will be more susceptible to drag perturbations than a more massive satellite) in accordance with Newton's Second Law. An effective or average value for the mass over the period of interest can be used as long as the actual mass does not vary greatly from this value.

The area the satellite presents to the atmosphere depends on the size, shape and orientation of the satellite. Uncontrolled tumbling or controlled attitude changes will cause a change in the presented area.

Either of these can be complex functions of time and/or orbital position. Again, an average or effective value must be employed.

Due to the long mean free path lengths associated with the molecular densities encountered at orbital altitudes, Newtonian flow theory is used in determining the coefficient of drag. In this model of gas dynamics the shock waves are considered to remain very close to the leading edge of the satellite, so each molecule acts independently, with no "knowledge" of any other molecule. Several major assumptions in this model are:

1) The satellite is assumed to be at rest, with the molecules flowing past with some relative velocity plus some distribution of a thermal velocity.

2) Each molecule will impinge upon the satellite and be momentarily retained before being re-emitted.

3) Collisions between incident and re-emitted molecules are neglected. Some broad assumptions must be made in evaluating this coefficient, but several sources recommend setting $2.0 \leq C_D \leq 2.2$ [8: 15; 9: 2-4].

Atmospheric Density. The single most important characteristic of the atmosphere's role in determining satellite lifetime is density. The atmospheric density is a function of time, solar activity, and altitude. As the planet revolves about its axis the sun warms the atmosphere, causing it to expand and form a "diurnal bulge" about two hours after midday. Although this causes relatively little change in density at low altitudes, density can increase by a factor of 8 at higher altitudes. The

27 day rotation period of the sun causes another periodic effect on the density. The position of the planet on its orbit provides another oscillation, with minima at apohelion and maxima at perihelion. Solar activity is related to the 11 year sunspot cycle, and this also affects atmospheric heating. Solar activity also varies essentially randomly from day to day with short term flares and other activity.

The primary assumption made in modelling the atmosphere, and the greatest simplification, is that density is a function only of altitude above some reference ellipsoid (geodetic altitude). While the factors mentioned in the preceding paragraph all cause deviations from this model, empirical data from actual satellite trajectories indicates density can be modelled as a function only of geodetic altitude reasonably accurately [14: 2; 8: 22]. Density drops off with altitude in accordance with the perfect gas law:

$$P = \rho \frac{R^*}{M} T \tag{17}$$

(where P is the pressure, M is the mean molecular weight of the atmosphere, T is temperature and R^* is the universal gas constant) and the hydrostatic equation:

$$d\rho = -\rho g dr \tag{18}$$

Extensive studies of earth satellites have shown a good first approximation of the density can be obtained by use of an exponential atmosphere model. This atmospheric model assumes the density drops off exponentially with altitude h:

$$\rho = \rho_o e^{(h_o - h)/H} \tag{19}$$

where ρ_o is the density at some reference altitude h_o, and H is the scale height (the distance over which density will change by a factor of e). Several types of exponential atmospheres exist, with the primary difference being in the determination of the scale height at the altitude of interest. Some of the methods of determining scale height are:

1) Strictly Exponential Atmosphere: The scale height is be considered to be constant over all altitudes.

2) Locally Exponential Atmosphere: The scale height is considered to be constant over some small altitude interval.

3) βr Constant Atmosphere: The product of the inverse of the scale height (β, not to be confused with ballistic coefficient) and the radius considered constant.

4) Isothermal atmosphere: The temperature is considered constant over some altitude interval. This leads to the quantity βr^2 being constant [14: 4].

Each of these methods is preferable in some situations. This model uses a constant scale height atmosphere, with the scale height set to the proper value for the region in which the satellite is expected to operate. The actual scale height used is 22.48 km at a reference altitude of 250 km.

Ellipsoidal Altitude. Since the density is a function of ellipsoidal altitude, it is necessary to find ellipsoidal altitude as a function of latitude. Given a planet with ellipticity ϵ, the ellipsoidal altitude, h_ϕ, can be approximated by:

$$h_g = r - \sqrt{\frac{R_e(1-\epsilon^2)}{1-\epsilon^2\cos^2\phi}} \tag{20}$$

where ϕ is the geocentric latitude [9: 3-5].

Relative Velocity. The velocity $\mathbf{v}$ the satellite has with respect to the rotating atmosphere is the difference between the inertial satellite velocity ($\mathbf{v}_s$) and the velocity of the atmosphere at that point ($\mathbf{v}_a$):

$$\mathbf{v} = \mathbf{v}_s - \mathbf{v}_a \tag{21}$$

Finding the velocity of the atmosphere involves several assumptions. The atmosphere rotates at approximately the same rate as the planet near the surface, but this rate drops off with altitude. Assuming that the entire atmosphere rotates uniformly and at the same rate as the planet greatly simplifies matters. If the atmosphere is considered to rotate uniformly, and at the same rate as the planet, then the inertial velocity of the atmosphere at a point located at $\mathbf{r}_a$ is given by:

$$\mathbf{v}_a = \omega_a \times \mathbf{r}_a \tag{22}$$

with ω_a being the inertial rotation rate of the planet.

This model includes perturbations due to atmospheric drag. In fact, drag is the probably the single most significant factor in determining the lifetime of low orbiting satellites, and orbits for which drag is not the predominant perturbation will be considered beyond the scope of this work. The physical parameters of the satellite used in this model are presented in Appendix B.

Averaged Equations for Atmospheric Drag. Equations representing the average change in orbital elements over one period due to air drag

have been produced by Sterne [13]. These are presented in Equation (23), where E is the eccentric anomaly, $E_1 = (1 - e\cos E)$, $E_2 = (1 + e\cos E)$, n is the mean motion $((\mu/a^3)^{1/2})$, and $d = (\omega_a/n)\cos i(1-e^2)^{1/2}$.

$$\Delta a = -2\beta a^2 \int_0^{2\pi} \rho \frac{E_2^{3/2}}{E_1^{1/2}}\left(1 - d\frac{E_1}{E_2}\right)^2 dE$$

$$\Delta e = -2(1-e^2)\beta a \int_0^{2\pi} \rho \frac{E_2^{1/2}}{E_1^{1/2}}\left(1 - d\frac{E_1}{E_2}\right)$$

$$\times [\cos E - .5d(E_1)(2\cos E - e - e\cos^2 E)/(1-e^2)]dE$$

$$\Delta i = -.5(\omega_a/n)\beta a \sin i(1-e^2)^{-.5} \int_0^{2\pi} \rho E_1^{5/2} E_2^{1/2}\left(1 - d\frac{E_1}{E_2}\right) \qquad (23)$$

$$\times \{1 + \cos 2\omega E_1^{-2}[(2-e^2)\cos^2 E - 1 + 2e^2 - 2e\cos E]\}dE$$

$$\Delta\Omega = -.5(\omega_a/n)\beta a \sin 2\omega(1-e^2)^{-.5} \int_0^{2\pi} \rho(1 - e^2\cos^2 E)\left(1 - d\frac{E_1}{E_2}\right)$$

$$\times [2e^2 - 1 - 2e\cos E + (2-e^2)\cos^2 E]dE$$

$$\Delta\omega = -\cos i\,\Delta\Omega$$

These equations can be numerically integrated to find the average change in the orbital elements over one period due to atmospheric drag. As with the geopotential averaged equations, periodic effects will be averaged out.

Third Body Perturbations

Third Body Geometry. If a third body is close enough, or massive enough, its gravitational attraction can have an effect on the satellite's orbit. In cases where the third body is in a nearly circular orbit about the primary, or the primary is in a nearly circular orbit around the third body, the third body can be modelled as being in two-body motion around the planet, simplifying the process of finding the vector from the third body to the planet.

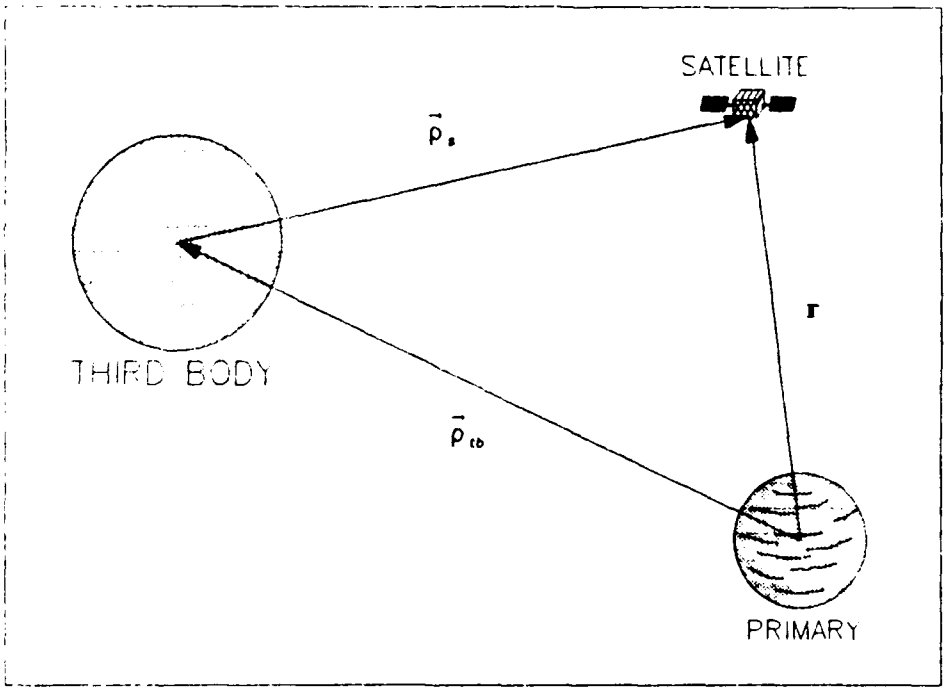

Figure 2. Third Body Geometry

Figure 2 shows the various position vectors involved. As indicated, the vector from the planet to the third body is given by $\vec{\rho}_{tb}$, and the

vector r locates the satellite from the center of mass of the planet. Hence, the vector from the third body to the satellite is given by $\vec{\rho}_s = \mathbf{r} - \vec{\rho}_{tb}$.

Gravitational Attraction. The effect a third body has on the orbit of a satellite is two-fold: 1) the satellite is affected by the attraction of the third body, perturbing its motion around the planet, and 2) the motion of the planet itself is affected. The acceleration due to the gravitational attraction of the third body in both cases is given by:

$$\mathbf{a} = -\mu_{tb}\frac{\vec{\rho}_{tb}}{\rho_{tb}^3} \tag{24}$$

where the vector from the third body to the body of interest is given by $\vec{\rho}_{tb}$ and μ_{tb} is the product of the mass of the third body and the universal gravitational parameter. The complete third body acceleration (including the direct effect of the third body on the satellite and the effect on the planet) is:

$$\mathbf{a}_{tb} = -\mu_{tb}\left(\frac{\vec{\rho}_s}{\rho_s^3} + \frac{\vec{\rho}_{tb}}{\rho_{tb}^3}\right) = -\mu_{tb}\left(\frac{(\mathbf{r} - \vec{\rho}_{tb})}{(r - \rho_{tb})^3} + \frac{\vec{\rho}_{tb}}{\rho_{tb}^3}\right) \tag{25}$$

This model includes third body effects from the sun [9: 3-4].

Averaged Equations for Third Body Effects. Kaufman [6] has developed equations representing the change in orbital elements over one period due to a third body. In the event that the inclination is equal to zero the equations for the change in inclination and longitude of ascending node are not valid. The subscript ($\odot$) indicates a parameter related to the third body. These equations are presented below.

$$\Delta n = 0$$

$$\Delta e = (-15\pi)(1-e^2)^{.5}(n_\odot/n)^2 e\alpha\beta(a_\odot/r_\odot)^3$$

$$\Delta i = -6\pi(n_\odot/n)^2(1-e^2)^{-.5}(\sin i)^{-1}(a_\odot/r_\odot)^3$$
$$\times[\alpha\delta(1+4e^2)+\beta\epsilon(1-e^2)-5\alpha\beta e^2\cos i]$$

$$\Delta\Omega = 6\pi(n_\odot/n)^2(1-e^2)^{-.5}(\sin i)^{-1}(a_\odot/r_\odot)^3 \qquad (26)$$
$$\times[\alpha\gamma(1+4e^2)\sin\omega+\beta\gamma(1-e^2)\cos\omega]$$

$$\Delta\omega = 6\pi(n_\odot/n)^2(1-e^2)^{-.5}(a_\odot/r_\odot)^3\times\Big\{(4\alpha^2-\beta^2-1)$$
$$-(\gamma\cos i/\sin i)(1-e^2)[\alpha(1+4e^2)\sin\omega+\beta(1-e^2)\cos\omega]\Big\}$$

The terms α, β, γ, δ and ϵ are coordinate frame conversion factors defined by:

$$\alpha = \vec{r}_\odot{}^\circ \cdot \vec{P}$$

$$\beta = \vec{r}_\odot{}^\circ \cdot \vec{Q}$$

$$\gamma = \vec{r}_\odot{}^\circ \cdot \vec{R}$$

$$\delta = \vec{r}_\odot{}^\circ \cdot \vec{P}'$$

$$\epsilon = \vec{r}_\odot{}^\circ \cdot \vec{Q}'$$

where

$$\vec{r}^\circ_\odot = \begin{bmatrix} \cos\Omega_\odot \cos\Phi_\odot \\ \sin\Omega_\odot \cos\Phi_\odot \\ \sin\Omega_\odot \cos\Phi_\odot \end{bmatrix}$$

$$\vec{P} = \begin{bmatrix} \cos\Omega\cos\omega - \sin\Omega\sin\omega\cos i \\ \sin\Omega\cos\omega + \cos\Omega\sin\omega\cos i \\ \sin i\cos\omega \end{bmatrix}$$

$$\vec{Q} = \begin{bmatrix} - \cos \Omega \cos \omega - \sin \Omega \sin \omega \cos i \\ - \sin \Omega \cos \omega + \cos \Omega \sin \omega \cos i \\ \sin i \cos \omega \end{bmatrix}$$

$$\vec{R} = \begin{bmatrix} \sin \Omega \sin i \\ - \cos \Omega \sin i \\ \cos i \end{bmatrix}$$

$$\vec{P}' = \begin{bmatrix} - \sin \Omega \cos \omega - \cos \Omega \sin \omega \cos i \\ \cos \Omega \cos \omega - \sin \Omega \sin \omega \cos i \\ 0 \end{bmatrix}$$

$$\vec{Q}' = \begin{bmatrix} \sin \Omega \cos \omega - \cos \Omega \sin \omega \cos i \\ - \cos \Omega \cos \omega - \sin \Omega \sin \omega \cos i \\ 0 \end{bmatrix}$$

As before, these equations can be used to obtain changes in the elements over one period due to the third body.

Solar Radiation Pressure.

Geometry. Any time the satellite is illuminated by the sun, solar radiation pressure exerts a slight but continuous force on it, producing a small acceleration. This is caused by the continuous momentum transfer from innumerable photon impacts. The acceleration depends on the area of the satellite, the mass of the satellite, the reflective characteristics of the satellite and the radiation pressure exerted by the sun at that distance. Figure 3 illustrates the various vector relations involved.

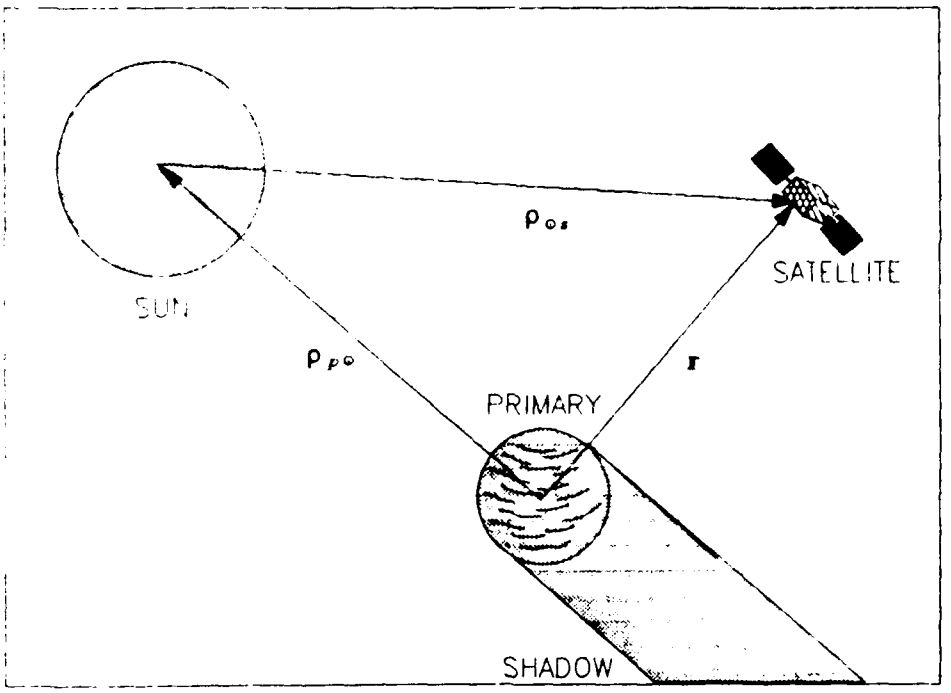

Figure 3. Solar Radiation Pressure Geometry

If the vector from the planet to the sun is ρ_{po} and the vector from the planet to the satellite is **r**, then the vector from the sun to the satellite

is $\rho_{os} = r - \rho_{po}$

The radiation pressure exerted is a function of distance from the sun alone, and, like gravity, is ruled by an inverse square law. Since the radiation pressure on a perfectly absorbing (black body) surface at the distance of the earth's orbit is known, it is convenient to express the absorptivity of the satellite as a ratio, and the distance from the satellite to the sun as a fraction of the distance from the earth to the sun.

The mean distance from the earth to the sun is 1 *AU*, or 149599650 km. Therefore, the solar radiation pressure at any other distance from the sun will be related to the pressure at 1 *AU* by the square of the product of the inverse of the distance and 1 *AU*. If the radiation pressure on a black body at 1 *AU* is P_R, then the pressure exerted on a black body at the satellite's position is $P_R\left(\frac{AU}{|\rho_{os}|}\right)^2$.

Reflectivity and Other Considerations. In reality, no satellite (or any other object) is a perfect black body. The reflectivity of the satellite can profoundly change the magnitude of the acceleration due to radiation pressure. The acceleration on a perfect reflector will be twice that on a perfect absorber, and a transparent satellite would feel no acceleration at all. Therefore a factor γ is included in the expression for the acceleration, where $\gamma = 1$ for a perfect absorber, $\gamma = 2$ for a perfect reflector, and $\gamma < 1$ for a translucent satellite, with real world satellites usually represented by values between 1 and 2. As an example, for aluminum $\gamma = 1.96$. The angle of reflection can affect the direction in which the acceleration is acting, but for simplicity it is justifiable to

assume the satellite reflects diffusely, resulting in the force pointing directly away from the sun.

The complete description of the acceleration due to solar radiation pressure is now:

$$\mathbf{a}_{srp} = \gamma P_R \frac{A}{m}\left(\frac{AU}{|\rho_{os}|}\right)^2 \rho_{os} \qquad (27)$$

where A is the area illuminated, and m is again the satellite mass [1: 188].

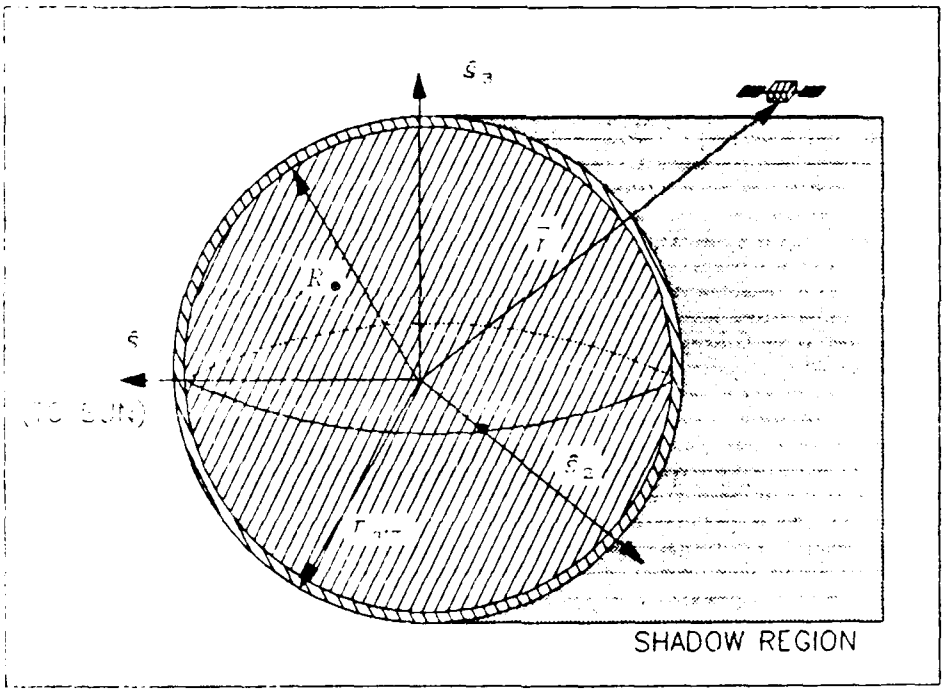

Figure 4. Occultation Geometry

Occultation. Note this acceleration only acts when the sun is illuminating the satellite -- during periods when the satellite is eclipsed or occulted it goes to zero. To check for planetary occultation, a planet

centered coordinate system is constructed with the first unit vector ($\hat{s}_1$) pointing in the direction of the sun (Figure 4). If the shadow cast by the planet is assumed to be a cylinder, and the satellite is located from the planet by the vector $\vec{r}$, the satellite will be occulted at any time that the following two conditions are both met:

$$\hat{s}_1 \cdot \vec{r} < 1$$

$$(\vec{r} \cdot \hat{s}_2)^2 + (\vec{r} \cdot \hat{s}_3)^2 \leq r_{atm}^2 \tag{28}$$

where r_{atm} is the radius of the planet plus the altitude to which the atmosphere can be considered to block solar radiation. Then at any time, the geometry of the sun-planet-satellite system can be checked for the presence of radiation pressure [10: 3-33]. Solar radiation pressure will be included in this model.

Averaged Equations for Solar Radiation Pressure. Cook [4] has derived equations for the rates of change of the orbital elements over one period. In these equations the effects of the primary's shadow are neglected.

$$\Delta a = 0$$

$$\Delta e = \frac{3(1-e^2)^{1/2}}{2na} T_p$$

$$\Delta i = -\frac{3W e \cos\omega}{2na(1-e^2)^{1/2}} \tag{29}$$

$$\Delta\Omega = -\frac{3W e \sin\omega}{2na(1-e^2)^{1/2}\sin i}$$

$$\Delta\omega = -\frac{3(1-e^2)^{1/2}}{2nae} S_p - \Delta\Omega$$

The terms S_p, S_p and W are components of the solar radiation force, and are defined by:

$$S_p = a_{srp}\left\{\left[\cos^2\frac{\zeta}{2}\cos(\omega+\Omega-\Lambda)+\sin^2\frac{\zeta}{2}\cos(\omega+\Omega+\Lambda)\right]\cos^2\frac{i}{2}\right.$$
$$+\left[\cos^2\frac{\zeta}{2}\cos(\omega-\Omega+\Lambda)+\sin^2\frac{\zeta}{2}\cos(\omega-\Omega-\Lambda)\right]\sin^2\frac{i}{2}$$
$$\left.+\frac{1}{2}[\cos(\omega-\Lambda)-\cos(\omega+\Lambda)]\sin i\sin\zeta\right\}$$

$$T_p = -a_{srp}\left\{\left[\cos^2\frac{\zeta}{2}\sin(\omega+\Omega-\Lambda)+\sin^2\frac{\zeta}{2}\sin(\omega+\Omega+\Lambda)\right]\cos^2\frac{i}{2}\right.$$
$$+\left[\cos^2\frac{\zeta}{2}\sin(\omega-\Omega+\Lambda)+\sin^2\frac{\zeta}{2}\sin(\omega-\Omega-\Lambda)\right]\sin^2\frac{i}{2}$$
$$\left.+\frac{1}{2}[\sin(\omega-\Lambda)-\sin(\omega+\Lambda)]\sin i\sin\zeta\right\}$$

$$h'\sin\omega = -\frac{a_{srp}}{2}\left\{[\cos(\omega+\Omega-\Lambda)-\cos(\omega-\Omega+\Lambda)]\sin i\cos^2\frac{\zeta}{2}\right.$$
$$+[\cos(\omega+\Omega+\Lambda)-\cos(\omega-\Omega-\Lambda)]\sin i\sin^2\frac{\zeta}{2}$$
$$\left.+[\cos(\omega+\Lambda)-\cos(\omega-\Lambda)]\cos i\sin\zeta\right\}$$

$$h'\cos\omega = \frac{a_{srp}}{2}\left\{[\sin(\omega+\Omega-\Lambda)-\sin(\omega-\Omega+\Lambda)]\sin i\cos^2\frac{\zeta}{2}\right.$$
$$+[\sin(\omega+\Omega+\Lambda)-\sin(\omega-\Omega-\Lambda)]\sin i\sin^2\frac{\zeta}{2}$$
$$\left.+[\sin(\omega+\Lambda)-\sin(\omega-\Lambda)]\cos i\sin\zeta\right\}$$

where a_{srp} is the magnitude of the acceleration due to solar radiation pressure described by Equation (27), ζ is the obliquity of the ecliptic,

and Λ is the geometric mean longitude of the sun, measured in the ecliptic. These equations may be used to find the secular and long period perturbations to the orbit due to solar radiation pressure.

Numerical Model

Two methods of applying all of the aforementioned perturbations in a mathematical model of satellite motion were considered -- an averaging method and Cowell's method. An averaging method would use the averaged equations presented at the end of each of the preceding sections (Equations (15), (23), (26) and (29)) to propagate the average orbital elements forward in time, giving a prediction of what the elements would be at the end of the 90 day period. Cowell's method would propagate the position and velocity of the satellite forward in time, subject to equations of motion found by summing the acceleration equations presented in each section (Equations (13), (16), (25) and (27)). Both methods have advantages, and both were investigated in making the selection.

Cowell's method of General Perturbations was chosen. In this method, the equations of motion for the satellite, including the perturbative accelerations, are expressed in rectangular coordinates and integrated numerically [12: 199]. This allows the use of the acceleration equations determined in each section, without requiring the averaged equations. The starting orbital elements are converted to a state vector in rectangular coordinates and used as initial conditions for the integration of the equations of motion. At each time step, the state vector is converted back to orbital elements so that they may be examined, if desired. This method has the advantages of being simple and straightforward, in addition to determining the actual position of the satellite at each time step. Its disadvantage is that it is slower

than methods which work with averaged orbital elements.

The equations for this model are of the form:

$$\dot{x} = v_x$$

$$\dot{y} = v_y$$

$$\dot{z} = v_y$$

$$\ddot{x} = \dot{v}_x = a_{gx} + a_{dx} + a_{tbx} + a_{srpx}$$

$$\ddot{y} = \dot{v}_y = a_{gy} + a_{dy} + a_{tby} + a_{srpy}$$

$$\ddot{z} = \dot{v}_z = a_{gz} + a_{dz} + a_{tbz} + a_{srpz} \qquad (30)$$

where a_g, a_d, a_{tb}, and a_{srp} are given in Equations (13), (16), (25), and (27), respectively. The motion is expressed in six first order equations to allow use of a fixed step size, eighth order Runge-Kutta integration algorithm described in reference [5].

III. Results

Search Method

Orbital elements on the Critical Surface were obtained by estimating an initial element set, propagating that orbit forward 90 days, and iteratively adjusting the estimate and repropagating the orbit to obtain a final value of periapsis altitude within a given tolerance of the decay threshold. This method was necessary because the numerical integration routine used was incapable of being operated backwards in time.

It was first necessary to determine realistic decay criteria. A decay threshold chosen too low resulted in very rapid decay at the 90 day point, making it very difficult to "fine tune" the initial semi-major axis such that on day 90 the periapsis altitude would be within a given tolerance of the decay threshold. If the decay threshold was too high, drag would not be the predominant perturbation, and the orbit would tend to not decay monotonically, with perturbations other than drag having a more pronounced affect on satellite lifetime.

Once a suitable threshold was determined, the initial estimate was obtained by computing the two-body semi-major axis for the desired periapsis altitude. Recalling Equation (3) from Chapter II:

$$r = \frac{a(1-e^2)}{1+e\cos(\nu)} \tag{31}$$

and recognizing that at perigee $\nu = 0$, the radius at perigee can be expressed as:

$$r_p = a(1 - e) \tag{32}$$

This initial estimate was then propagated forward through 90 days using the numerical method described in Chapter II. If the final periapsis altitude was not within the decay threshold tolerance, the semi-major axis was incrementally adjusted until the desired periapsis altitude was obtained. This procedure was repeated over a range of inclinations at each of five eccentricities. Due to the iterative nature of the search method, obtaining a single data point required between ten and fifteen, and sometimes as many as twenty, integrator runs. Since each 90 day integrator run required approximately twenty minutes of computer time, producing the Critical Curves was a very time intensive operation.

A polynomial fitting routine was then applied to the data to generate functions which would allow interpolation between the data points and simplify use of the Critical Curve at that eccentricity.

Decay Threshold

To establish a realistic decay threshold, general decay characteristics were examined at $e = .001$. For a given periapsis altitude, a less eccentric orbit will have a smaller semi-major axis than a more eccentric orbit, and will spend a larger fraction of the orbital period at lower altitudes where the satellite will be subjected to drag. Therefore, lower eccentricity orbits are more profoundly affected by drag, so a realistic threshold for low eccentricity should be acceptable for higher eccentricities. The behavior of the periapsis altitude over time for a typical orbit ($a_i = 6270km, e_i = .001, i_i = 45^\circ$) is shown in Figure 5.

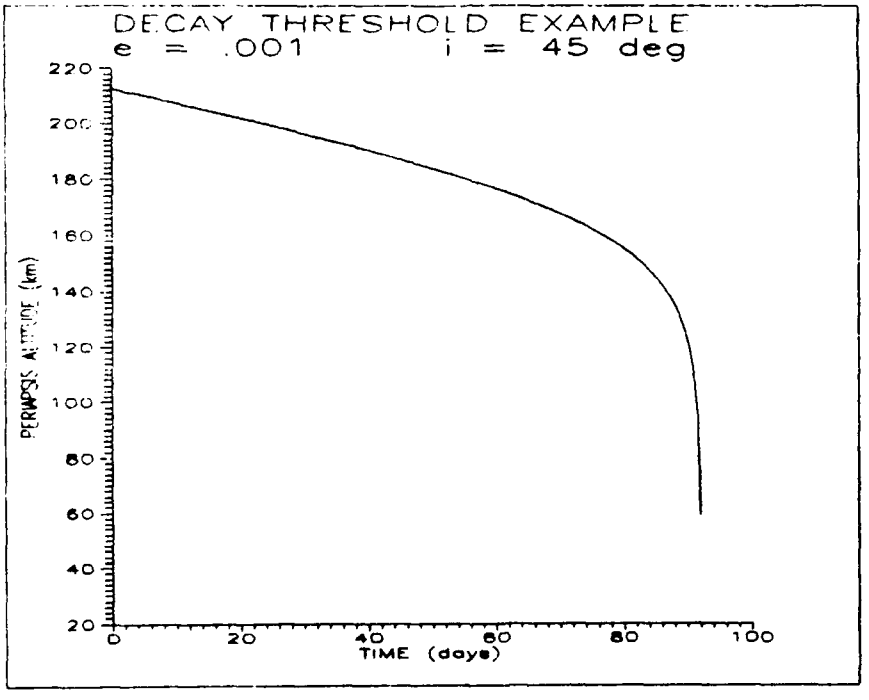

Figure 5. Terminal Orbital Decay

It can be seen that after a periapsis altitude of 150 km is reached, decay becomes very rapid. At periapsis altitudes below about 120 km, the curve is almost vertical. Attempting to determine initial conditions to result in a final periapsis altitude in this region would not only be very difficult, but the lifetime of any orbit in that regime would be extremely sensitive to variations in initial conditions and perturbative forces. Therefore, a minimum decay threshold of 130 km was selected. Two additional decay threshold altitudes were selected at 140 km and 150 km. The tolerance allowed was 10 km above the threshold. When the slope of the decay curve permitted, an effort would be made to obtain a final periapsis altitude as close to the threshold as possible.

Critical Curve Families

Eccentricity = .001 The smallest eccentricity examined was $e = .001$ to reflect the scarcity of perfectly circular orbits in real world situations. The curve family is shown in Figure 6.

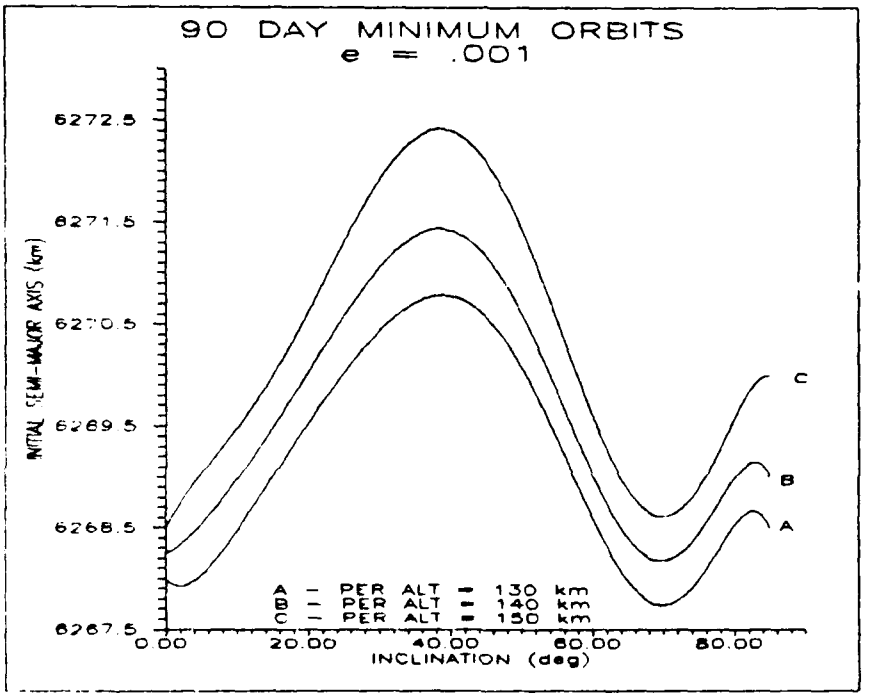

Figure 6. Critical Curve for e=.001

A high degree of inclination dependence can be seen in these curves, causing a variation in initial semi-major axis of nearly 5 km over the inclination range. This seems to indicate a much lower rate of decay at low and high inclinations than at mid-inclinations. A short investigation as to the nature and cause of this inclination dependence is included later in this chapter.

The polynomial fitting routine was unable to produce a good fit to the data with less than a seventh order polynomial, reflecting the relative complexity of the curve. The polynomial coefficients are given in Appendix C, Table C-1.

Eccentricity = .01 At $e = .01$ the inclination dependence is still obvious, although less pronounced. The curve family is shown in Figure 7.

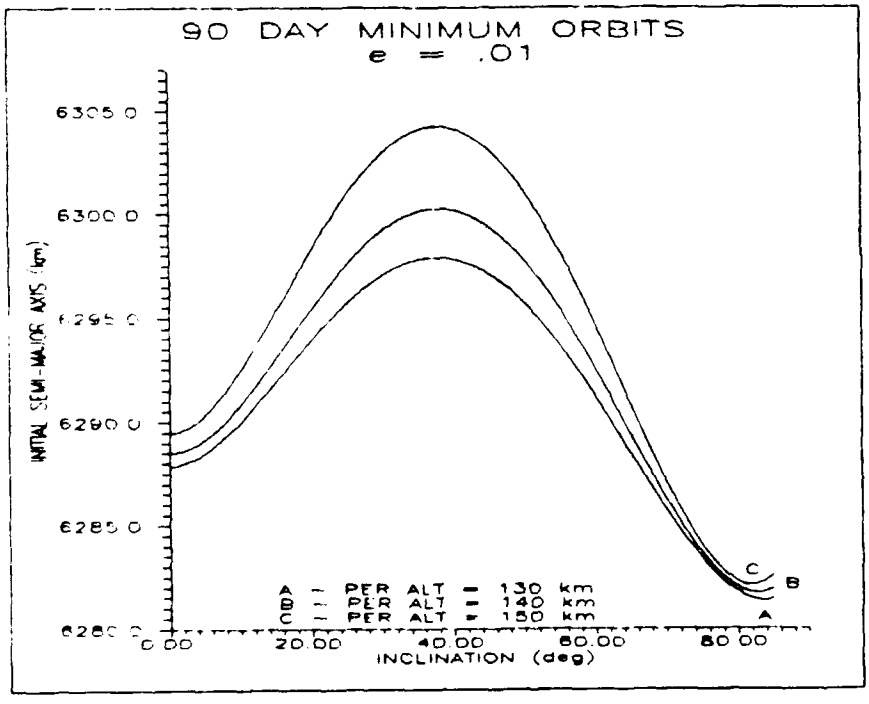

Figure 7. Critical Curve for e=.01

Although the inclination dependence produces a less striking effect in the shape of the curve at this eccentricity, the effect on the range of initial semi-major axis values is very noticeable, with almost 25 km of

variation.

The polynomial fitting routine produced a good fit to these data sets, and all of the following data sets, with a fourth order polynomial. The polynomial coefficients are given in Appendix C, Table C-2.

Eccentricity = .02 At $e = .02$ it was first seen that at higher inclinations (as before, corresponding to slower decay) periapsis altitude actually increased over the 90 day period.

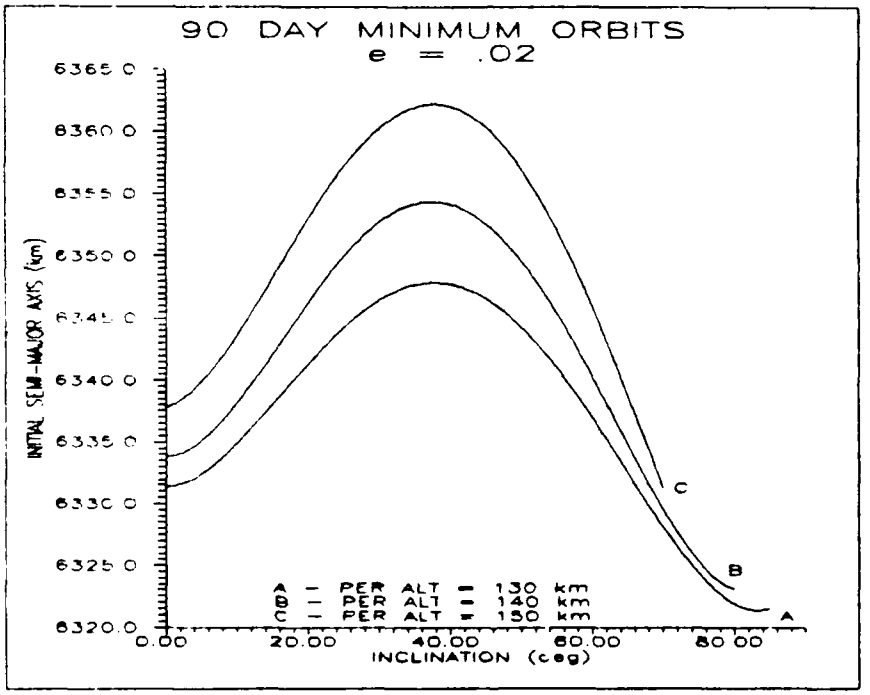

Figure 8. Critical Curve for e=.02

Data showing this tendency is not presented here, since it is not of interest in terms of short term drag-limited lifetime. This results in some of the fitted curves being clipped at higher inclinations. The

curves presented here are clipped at the first inclination where the final periapsis altitude is higher than the initial periapsis altitude. The curve family is shown in Figure 8. The trend towards increasing range of initial semi-major axis values continued, spanning almost 45 km in this case.

The polynomial fit was again accomplished with a fourth order polynomial. The polynomial coefficients are given in Appendix C, Table C-3.

Eccentricity = .04 At $e = .04$ the tendency mentioned in the last section became more pronounced, requiring further clipping of the curves. The curve family is shown in Figure 9.

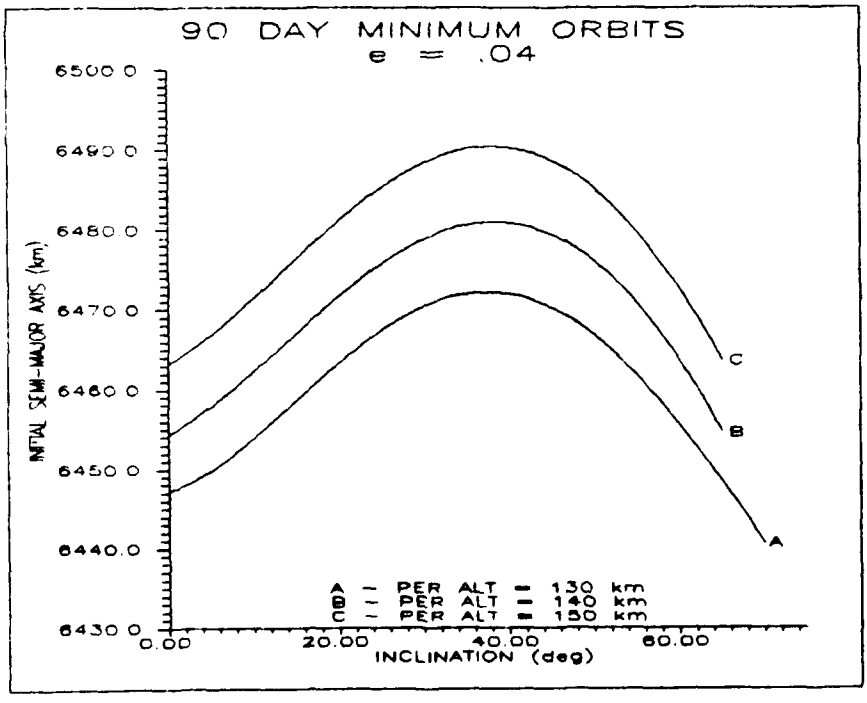

Figure 9. Critical Curve for e=.04

The trend towards a wider spread in initial semi-major axis seemed to have leveled off at just over 50 km in this and the next graph, but this can largely be attributed to the data clipping. The tendency for periapsis altitude to "climb" at high inclinations would significantly increase the range, were the higher inclinations to be included.

The polynomial coefficients for these curves are given in Appendix C, Table C-4.

Eccentricity = .1 The largest eccentricity examined was $e = .1$. The curve family is shown in Figure 10.

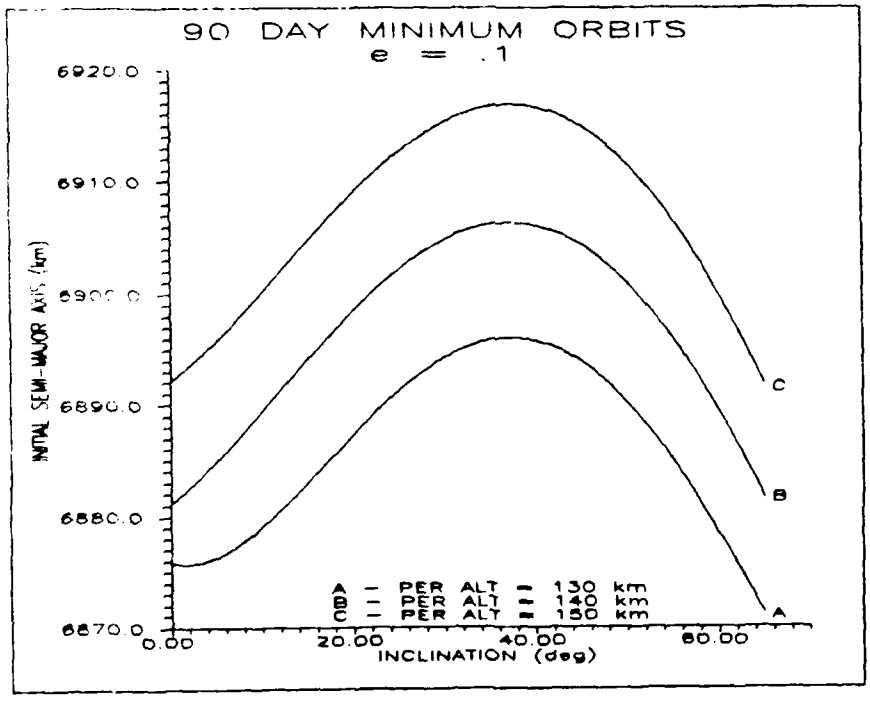

Figure 10. Critical Curve for e=.1

It is obvious that at this and larger eccentricities, smaller inclination ranges will "decay down" to a final periapsis altitude. At these eccentricities, drag will be less of a factor in determining lifetime, so these will no longer be short term, low orbiting satellites.

Again, a fourth order polynomial was sufficient. The polynomial coefficients are given in Appendix C, Table C-5.

Note that in this section, the x-axis represents initial semi-major axis, so "peaks" on these graphs are indicative of higher amounts of decay.

Inclination Dependence

To investigate the cause of the inclination dependence noted in the graphs above, the model was run for 90 days in five different configurations. In four of the trials, all of the perturbations but one were zeroed out. In the fifth all of the perturbations were zeroed out. The initial conditions used were considered to be representative of the range of initial conditions considered in determining the Critical Curves. The five curves presented in these graphs represent the final perigee altitude, as a function of inclination, for each of the separate perturbations and the unperturbed case. The no perturbation case differs from the initial perigee altitude by only the integrator error. These graphs depict final periapsis altitudes, so the "peaks" represent minimal decay, the opposite of the previous section.

As can be seen from Figure 11, the inclination dependence at middle eccentricities resides almost entirely in the geopotential perturbation. The drag perturbation causes the same total decay at all inclinations. This is different than would be the case for the earth, where the equatorial bulge in the planet is mirrored in an equatorial bulge in the atmosphere (and in the ellipsoidal altitude density model used here) and drag perturbations are therefore inclination dependent, with low inclinations being more affected by drag. Because Venus is much more spherical than earth, there is no significant corresponding equatorial bulge. The solar third body perturbation seems to be negligible, having less of an effect than even the solar radiation pressure. The radiation pressure perturbation causes a slight inclination dependence, with

maximum effect near 20 degrees of inclination. Neither radiation pressure nor third body effects are normally considered to be significant for low orbiting satellites, but were included here because of Venus' proximity to the sun.

Figure 12 presents the same data as Figure 11, but for the low eccentricity case. In this case, the same observations can be made concerning solar radiation pressure and third body effects. These could be expected to have even less of an effect in this lower orbit. The drag, as expected, is much more predominant for this lower orbit, and is again independent of inclination. The geopotential effect is significantly different, with almost no tendency to cause the orbit to "climb."

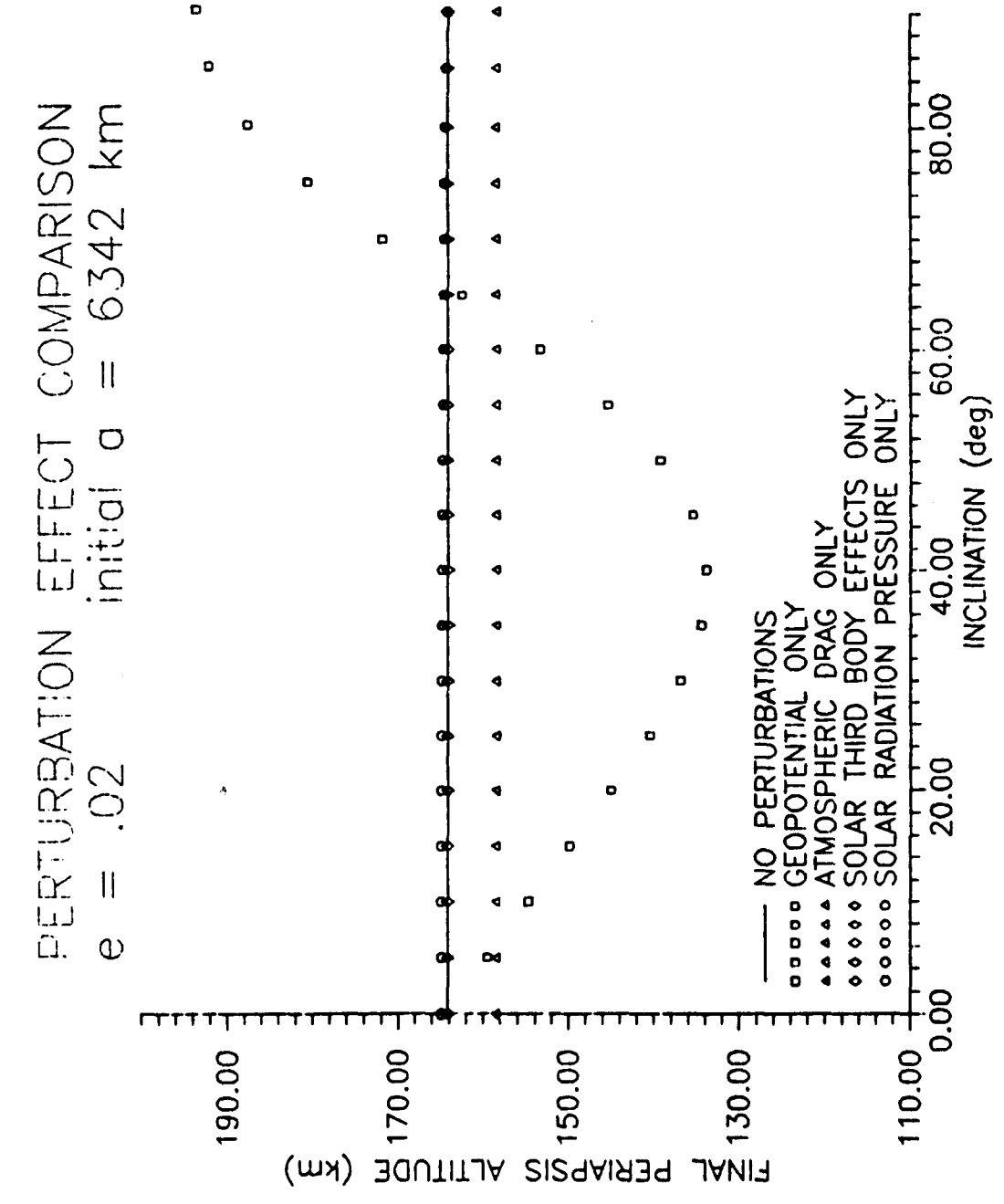

Figure 11. Final Periapsis Altitude as a Function of Inclination (e=.02)

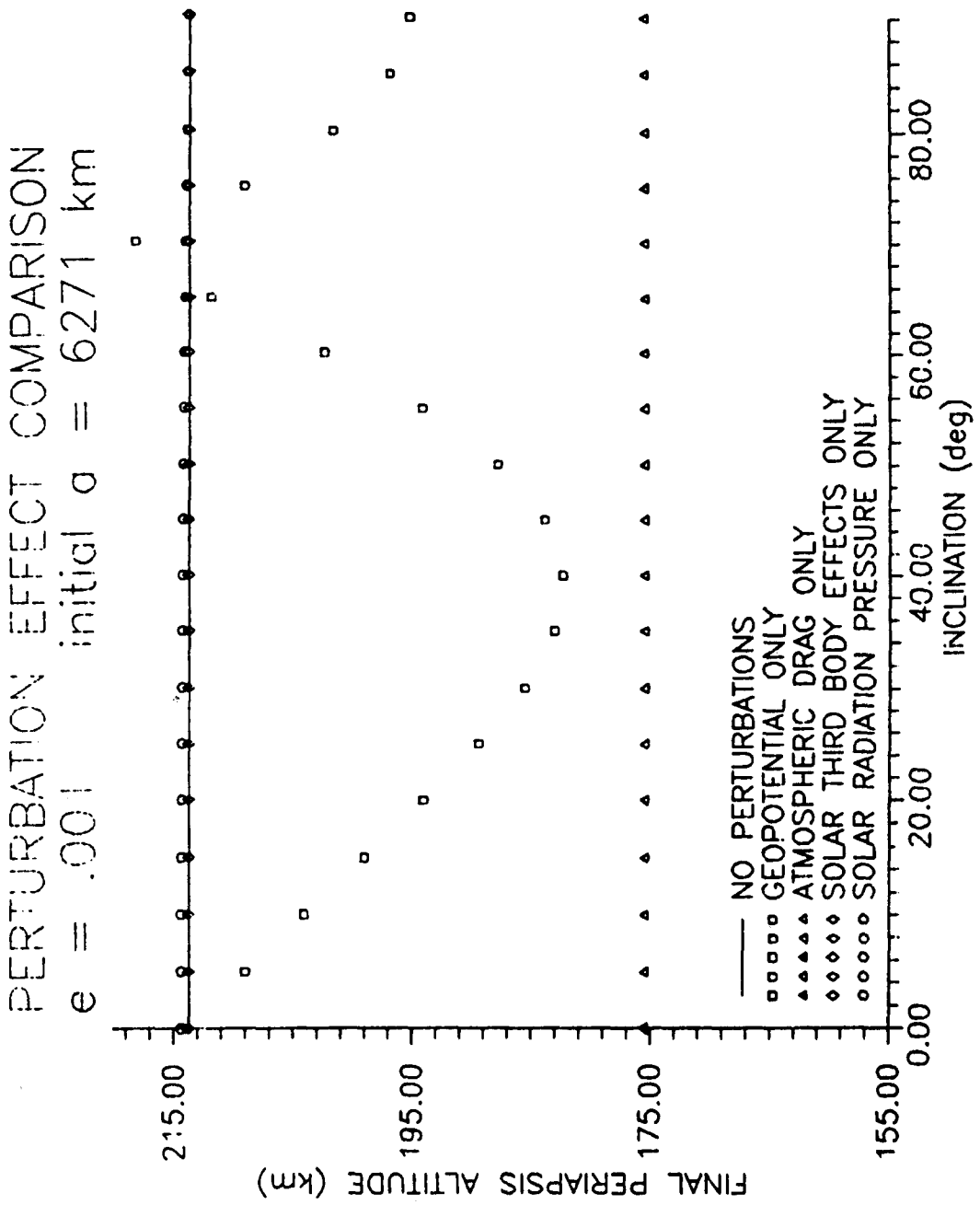

Figure 12. Final Periapsis Altitude as a Function of Inclination (e=.001)

Geopotential Perturbation Cyclic Effects

Since the geopotential produces a conservative force, it could be expected that the dependence seen in Figures 11 and 12 would be part of a cyclic behavior. To investigate this hypothesis, longer (120 day) simulations at the previously investigated eccentricities of .02 and .001 were run.

High Eccentricity. Inclinations used for the higher eccentricity case were 40 degrees (where the gravity perturbation leads to the fastest decay), 65 degrees (where the gravity perturbation has a minimal effect), and 85 degrees (where the gravity perturbation seems to actually make the periapsis altitude increase).

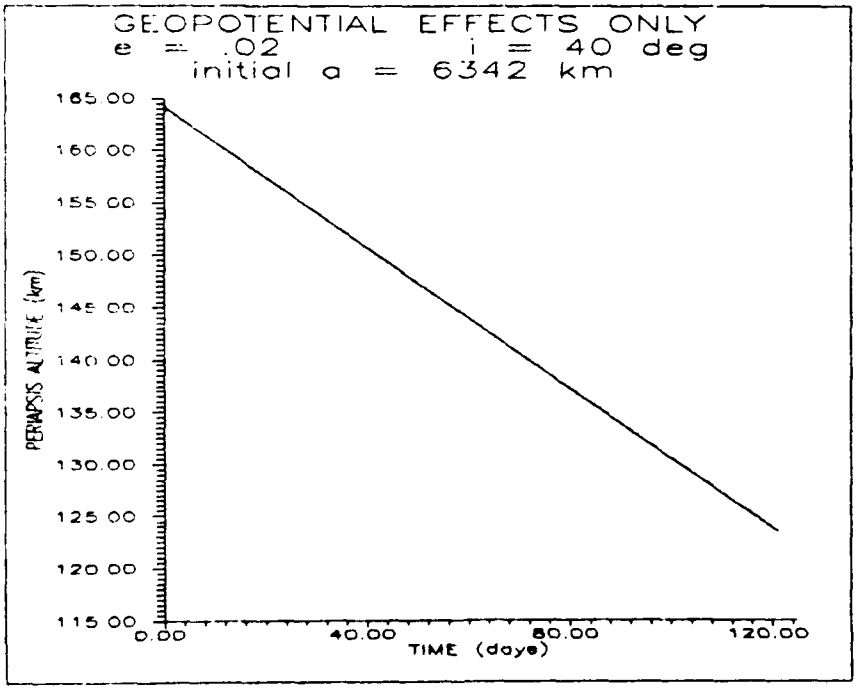

Figure 13. Periapsis Altitude as a Function of Time

Figure 13 shows the effect geopotential has on periapsis altitude. As could be expected from Figure 11, this shows up as a decrease in periapsis altitude. The expected periodicity (due to geopotential producing a conservative force) is not apparent, however. Note that in these graphs, like Figures 11 and 12, the final periapsis altitude is plotted, so lower parts of the curve correspond to more decay.

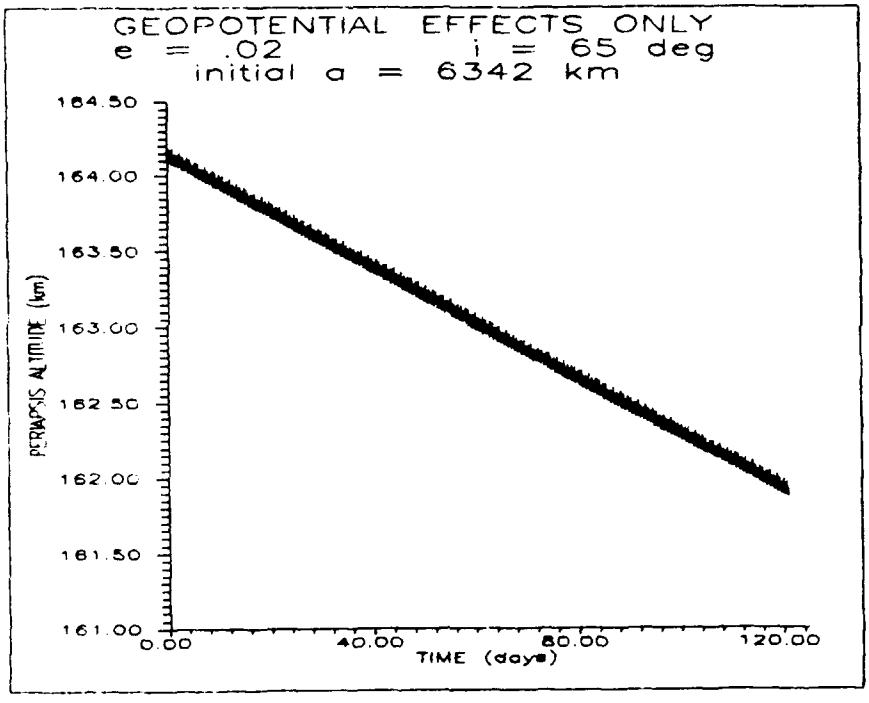

Figure 14. Periapsis Altitude as a Function of Time

In Figure 14 the geopotential effect over the 120 day period shows up as a small net change (note the scale -- Figures 13 and 14 are to different scales) with a short period oscillation superimposed. This is consistent with the results shown in Figure 10, where there was very

little decay at 65 degrees inclination. This short period oscillation would also show up in Figure 13 but is lost on that graph because its magnitude is so much smaller than that of the "net" change.

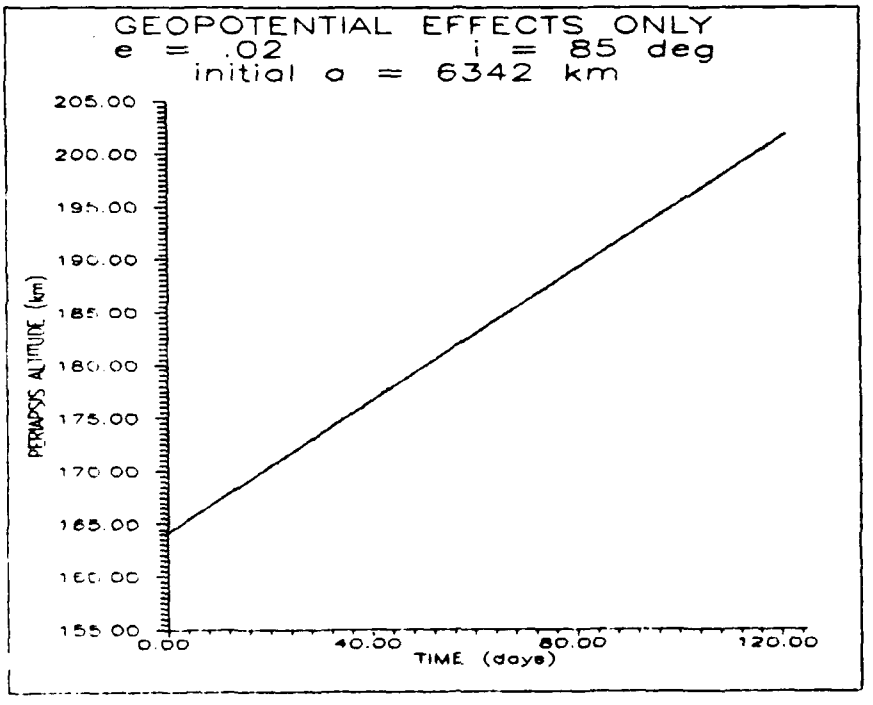

Figure 15. Periapsis Altitude as a Function of Time

In Figure 15 the expected "climb" in periapsis altitude can be seen. All three of these figures show some magnitude of net change over the 120 days, along with some small fast oscillation. In no case does the larger net change give evidence of being periodic.

Low Eccentricity. Inclinations used for the low eccentricity case were 40 degrees (where the most decay occurred), 65 degrees (where the geopotential had minimal effect), and 70 degrees (where the geopotential caused a small increase in periapsis altitude). The results are presented in Figures 16, 17, and 18.

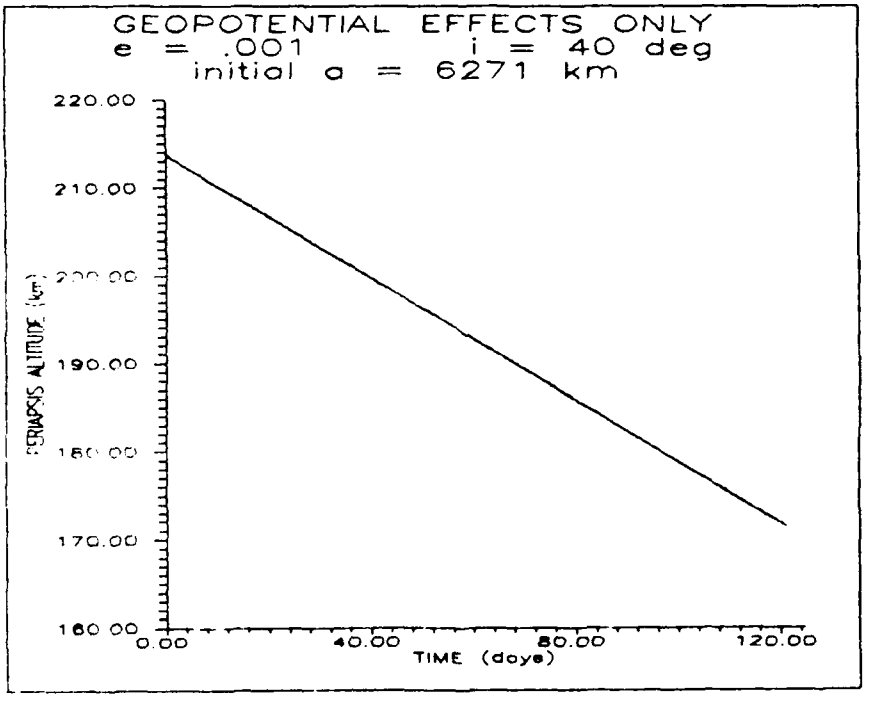

Figure 16. Periapsis Altitude as a Function of Time

Figure 16 is very similar to Figure 13, showing the overall drop in periapsis altitude, consistent with Figure 12.

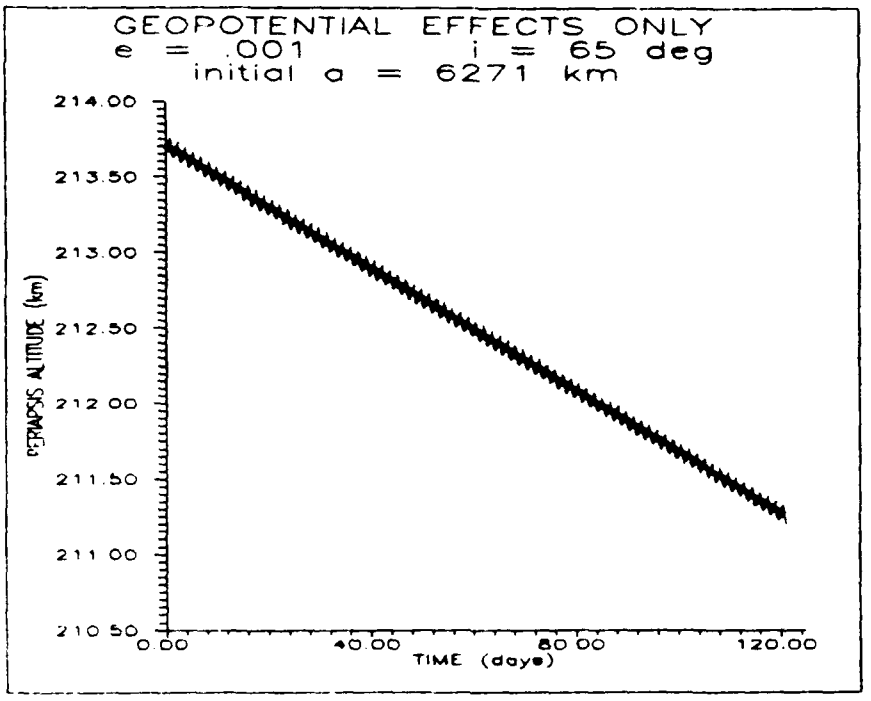

Figure 17. Periapsis Altitude as a Function of Time

In Figure 17 the small net change is again seen, with the expected small fast oscillation visible because of the scale of the graph.

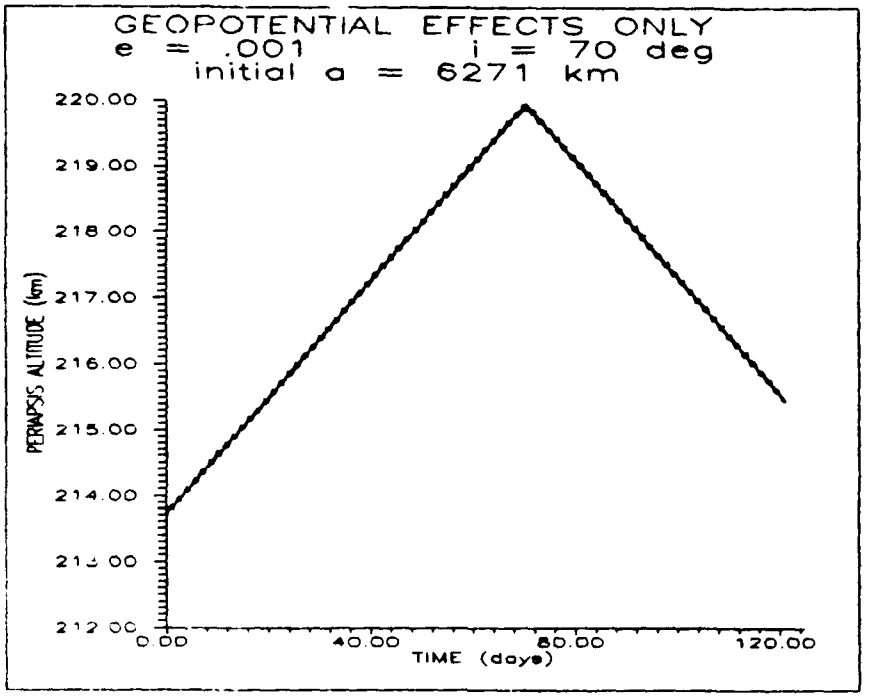

Figure 18. Periapsis Altitude as a Function of Time

In Figure 18, evidence of the expected periodicity in periapsis altitude is finally seen. Because this curve represents the relatively small "climb" in periapsis altitude seen at low eccentricity, the short period oscillation is more noticeable than in Figure 15. These figures, taken together, show that the effect of geopotential seen with this model is periodic, as predicted by the fact that the geopotential produces a conservative force. The response is composed of multiple oscillations of differing periods. This investigation implies that the inclination of 65 degrees is relatively stable for the periapsis altitude for Venus. This is accompanied by relative stability in semi-major axis and eccentricity, with changes in these elements for both examined eccentricities of less

than .25 km and .0004, respectively, over the 120 day period. Satellites placed in 65 degree inclination orbits would experience minimal change in periapsis altitudes, at least within the 120 day time frame examined. It should be possible to adjust the inclination so that geopotential induced "climb" will offset the drag induced decay in the periapsis, at higher altitudes, resulting in short term orbits with roughly constant periapsis altitudes.

Critical Surfaces

Visual representations of the three Critical Surfaces were produced with the aid of a three-dimensional plotting program. These plots are presented as Figures 19, 20 and 21.

Note that in these plots, inclination runs along the nearest axis, increasing from left to right. Eccentricity (multiplied by 1000 for scaling) is plotted along the other horizontal axis, increasing from front to back. The vertical axis represents the difference between initial semi-major axis and the planetary radius.

The Critical Curves can be seen as the lines of constant eccentricity corresponding to the values discussed earlier. Other values on the surface are interpolations of the plotting program. Obviously, more data would significantly increase the accuracy of these surfaces, but the trend of the data is apparent. The plotting program also interpolates over regions where the data has been clipped at higher eccentricities and inclinations.

Any set of orbital elements corresponding to a point above these Critical Surfaces will produce an orbit which will not decay below the specified minimum altitude in 90 days.

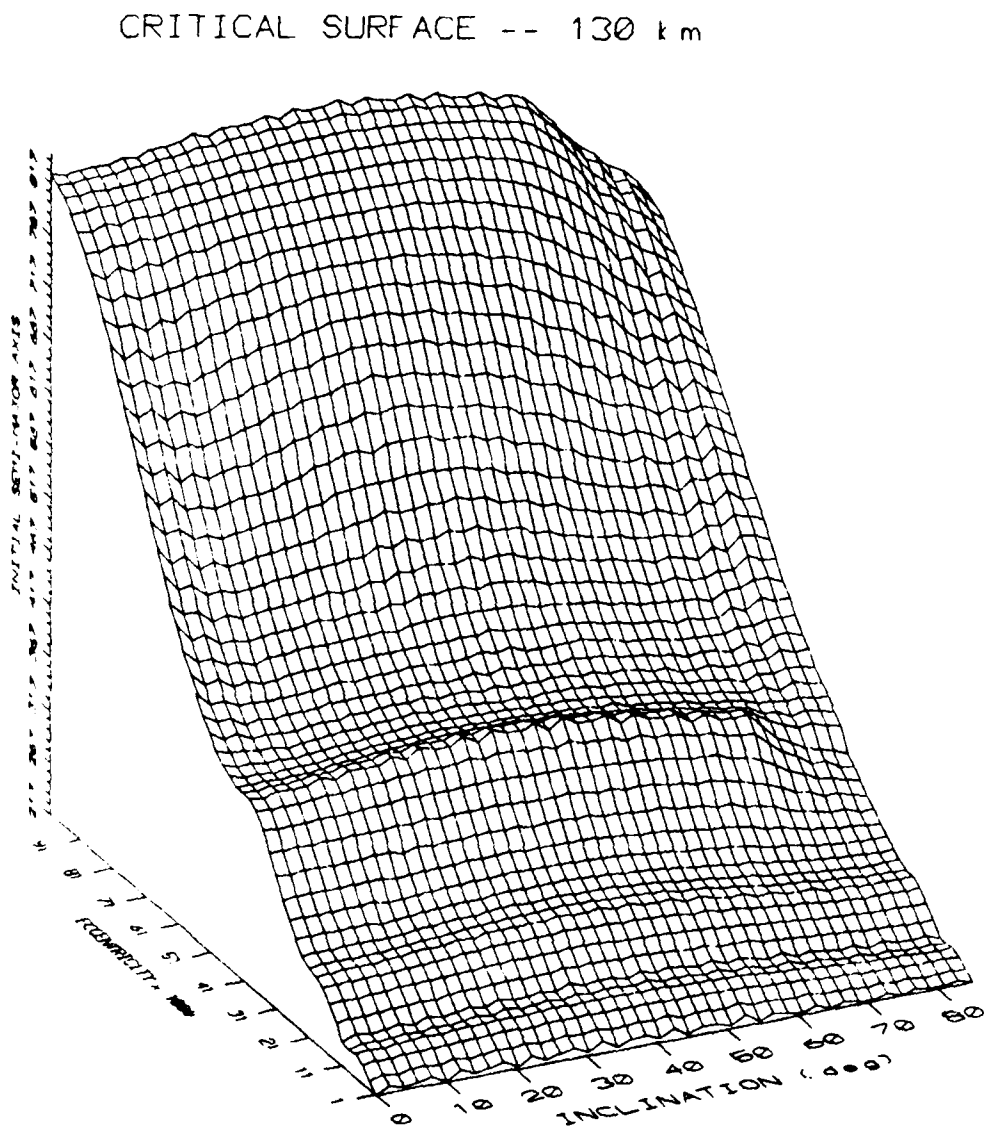

Figure 19. Critical Surface (Final Periapsis Altitude = 130 km)

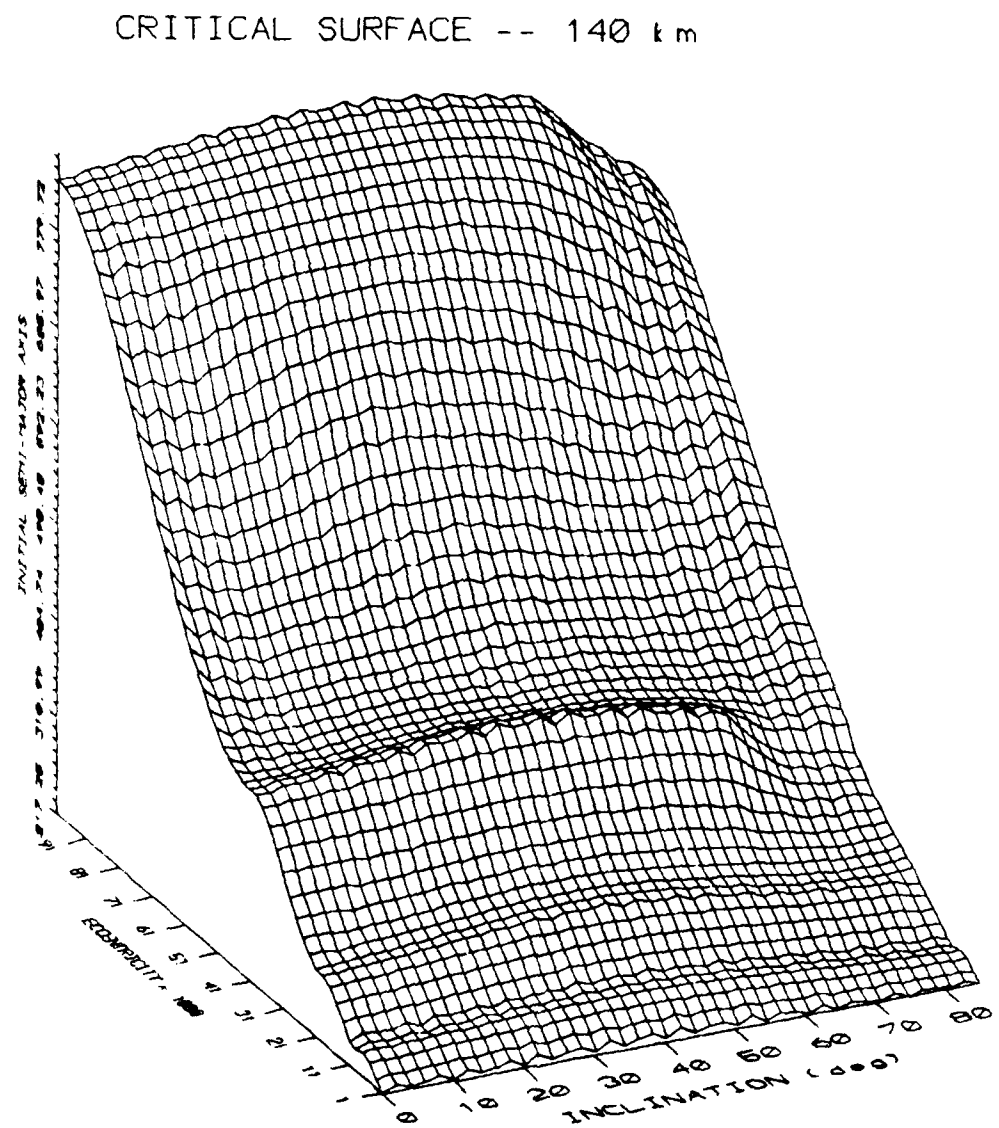

Figure 20. Critical Surface (Final Periapsis Altitude = 140 km)

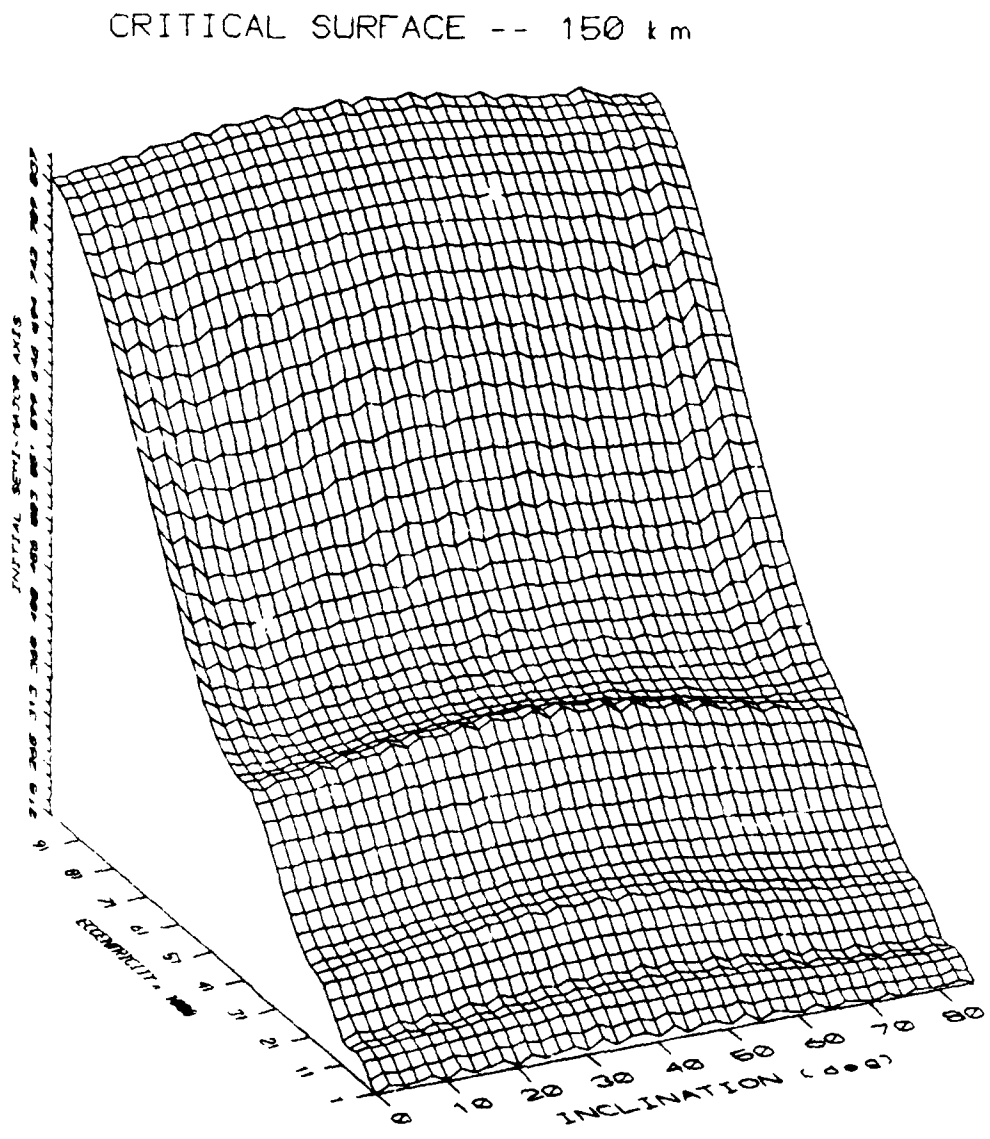

Figure 21. Critical Surface (Final Periapsis Altitude = 150 km)

IV. Conclusions and Recommendations

Critical Surfaces can be produced with an iterative numerical method. These surfaces show a strong geopotential-caused inclination dependence which is periodic in nature. Critical Surfaces generated for lifetimes in excess of 90 days would be more effected by this long term periodicity. Drag, as expected, causes a uniform decay rate at all inclinations when considered for a spherical planet. Although neither solar third body effects nor radiation pressure made substantial contributions to the rates of decay, solar radiation pressure did have a small effect, and would probably be significant for higher orbits because of Venus' proximity to the sun.

At certain inclinations and eccentricities the periodic geopotential effect takes the form of an increase in periapsis altitude. This could be used to offset the decay due to drag for some finite time, in order to maintain a constant periapsis altitude. This possibility should be investigated more closely. For high eccentricity and inclination, the geopotential effect offset the drag decay completely, resulting in orbits which were not lifetime-limited by decay in the time frame examined. Since the geopotential effect is periodic, these orbits would have finite lifetimes, but this effect could be used in conjunction with limited station-keeping, and this also should be investigated.

This investigation only considered zonal harmonics up to sixth order. Further investigation involving sectoral and tesseral harmonics could be conducted, but would require consideration of all six orbital

elements, complicating analysis.

As mentioned in the Introduction, perhaps the most interesting application of this type of investigation would be for lightsat mission planning. Interplanetary exploration probes are not likely to be short-term expendable spacecraft in the near future, but the military potential of small, inexpensive, single purpose satellites is great. Producing the Critical Surfaces for these types of missions would require the inclusion of third body effects from the moon, which would add complexity to the surfaces. This area of research should be pursued.

Appendix A

Physical Constants for the Planet Venus

The physical constants for the primary used in this model were taken from References 9 and 10.

Mean Distance from the Sun	108100000 km
Planetary Radius (R_*)	6051 km
Occultation Radius (r_{atm})	6141 km
μ_*	3.24858 E 5 km^3/sec^2
Rotation Rate (ω_*)	-1.71 E -5 deg/sec
Planetary Ellipticity (ϵ)	0.0
Scale Height (β)	22.48 km
Reference Height	250 km
Reference Density	3.19 E -4 kg/km^3

Geopotential Coefficients

J_2	-.45207 E -5
J_3	.13421 E -5
J_4	.24135 E -5
J_5	.25940 E -6
J_6	.33613 E -6

Appendix B

Physical Parameters of the Spacecraft for this Model

The physical parameters for the spacecraft for this model were loosely based on those for the Magellan Venus Orbiter (Reference 9).

Spacecraft Mass (m)	1085 kg
Coefficient of Drag (C_d)	2.0
Spacecraft Area (A)	24 m^2
Reflectivity Factor (γ)	1.0

Appendix C

Polynomial Coefficients for the Critical Curves

The coefficients for the polynomials fitted to the Critical Curve data are given in Table C-1 through C-5.

Table C-1. Critical Curve Polynomial Coefficients for e=.001

DEGREE	DECAY THRESHOLD (Periapsis Altitude)		
	130 km	140 km	150 km
0	6267.99	6268.24	6268.49
1	-6.95906 E-2	2.99023 E-2	1.32518 E-1
2	2.08757 E-2	7.38482 E-3	-7.20412 E-3
3	-1.28716 E-3	-4.75775 E-4	4.50068 E-4
4	4.49841 E-5	2.08839 E-5	-6.96061 E-6
5	-8.90591 E-7	-5.18589 E-7	-9.0554 E-8
6	8.79975 E-9	5.92692 E-9	2.63286 E-9
7	-3.33571 E-11	-2.45627 E-11	-1.44104 E-11

Table C-2. Critical Curve Polynomial Coefficients for e=.01

DEGREE	DECAY THRESHOLD (Periapsis Altitude)		
	130 km	140 km	150 km
0	6287.83	6288.54	6289.48
1	1.77987 E-2	-2.62089 E-2	-9.69216 E-3
2	2.62497 E-2	3.32471 E-2	4.07476 E-2
3	-6.79421 E-4	-8.40906 E-4	-1.04491 E-3
4	4.20771 E-6	5.20687 E-6	6.53673 E-6

Table C-3. Critical Curve Polynomial Coefficients for e=.02

DEGREE	DECAY THRESHOLD (Periapsis Altitude)		
	130 km	140 km	150 km
0	6331.34	6333.85	6337.94
1	2.75642 E-2	-4.46667 E-3	8.94402 E-2
2	4.31136 E-2	5.70271 E-2	6.14433 E-2
3	-1.11557 E-3	-1.4776 E-3	-1.61977 E-3
4	6.92373 E-6	9.3038 E-6	1.01088 E-5

Table C-4. Critical Curve Polynomial Coefficients for e=.04

DEGREE	DECAY THRESHOLD (Periapsis Altitude)		
	130 km	140 km	150 km
0	6447.23	6454.59	6463.24
1	3.03818 E-1	4.0992 E-1	5.80655 E-1
2	4.82529 E-2	4.42407 E-2	3.25586 E-2
3	-1.32737 E-3	-1.23606 E-3	-9.41725 E-4
4	7.95499 E-6	7.12796 E-6	4.68943 E-6

Table C-5. Critical Curve Polynomial Coefficients for e=.1

DEGREE	DECAY THRESHOLD (Periapsis Altitude)		
	130 km	140 km	150 km
0	6875.97	6882.02	6891.97
1	-2.89251 E-1	2.33786 E-1	6.39414 E-1
2	7.58337 E-2	5.74248 E-2	2.77024 E-2
3	-1.87211 E-3	-1.60948 E-3	-9.46644 E-4
4	1.16795 E-5	1.02871 E-5	5.81199 E-6

References

1. Baker, Robert M.L., Jr. Astrodynamics. New York: Academic Press, 1967.

2. Bate, Roger R., Donald D. Mueller, and Jerry E. White. Fundamentals of Astrodynamics. New York: Dover Publications, 1971.

3. Cain, Christina L. Orbits Containing Arcs of Minimum Altitude Variation. MS thesis, AFIT/GA/ENY/89J-1. School of Engineering, Air Force Institute of Technology (AU), Wright-Patterson AFB OH, 1989.

4. Cook, G. E., and Janice M. Hughes. "The Orbits of Needle Satellites," Planetary and Space Science, Vol. 9, p. 153, 1962.

5. Fehlberg, E. "Classical Fifth-, Sixth-, Seventh-, and Eighth-Order Runge-Kutta Formulas with Stepsize Control," NASA TR R-287, October 1968.

6. Kaufman, Bernard. "Variation of Parameters and the Long-Term Behavior of Planetary Orbiters," AIAA Paper No. 70-1055, AAS/AIAA Astronautics Conference, 1-3 August 1970.

7. Kaula, William K. Theory of Satellite Geodesy. Waltham, Mass: Blaisdell Publishing Company, 1964.

8. King-Hele, Desmond. Theory of Satellite Orbits in an Atmosphere. London: Butterworths, 1964.

9. Kwok, Johnny H. The Artificial Satellite Analysis Program (ASAP). Jet Propulsion Laboratory, 20 April 1987.

10. Kwok, Johnny H. The Long-Term Orbit Predictor (LOP). Jet Propulsion Laboratory, 30 June 1986.

11. Merson, R. H. "The Motion of a Satellite in an Axi-Symmetric Gravitational Field," Geophysical Journal, Vol. 4, p. 17, 1961.

12. Roy, Archie E. Orbital Motion. Bristol: Adam Hilger Ltd, 1982.

13. Sterne, Theodore E. "Effect of the Rotation of a Planetary Atmosphere Upon the Orbit of a Close Satellite," ARS Journal, Vol. 29, No. 10, p. 777, 1959.

14. Vinh, Nguyen X., Adolf Buseman, and Robert D. Culp. Hypersonic and Planetary Entry Flight Mechanics. Ann Arbor: The University of Michigan Press, 1980.

15. Zendell, Alan, Richard D. Brown, and Samir Vincent. NASA Space Vehicle Design Criteria (Environment): Gravity Fields of the Solar System. NASA SP-8117, April 1975.

Vita

Captain Jeff Smith entered the United States Air Force Academy in 1982, and graduated with a Bachelor of Science in Astronautical Engineering. In July 1986 he was assigned to the Atlas Satellite Launch Division of the 6595th Aerospace Test Group, Vandenberg AFB, California, as a Launch Systems Engineer. During his three year assignment he served as a member of the processing and launch team for five Atlas launches, including two as Assistant Launch Control Officer and one as Launch Control Officer. He also met his future wife, Lieutenant (now Captain) [redacted]. He was assigned to AFIT in May of 1989.

PERMANANT ADDRESS:

[redacted]

REPORT DOCUMENTATION PAGE

Form Approved
OMB No 0704-0188

1. AGENCY USE ONLY (Leave blank)	2. REPORT DATE	3. REPORT TYPE AND DATES COVERED
	26 Nov 90	MS Thesis

4. TITLE AND SUBTITLE
Minimum Orbits About the Planet Venus

5. FUNDING NUMBERS

6. AUTHOR(S)
Jeffrey J. Smith, Capt, USAF

7. PERFORMING ORGANIZATION NAME(S) AND ADDRESS(ES)
School of Engineering
Air Force Institute of Technology (AU)
Wright-Patterson AFB, OH 45433-6583

8. PERFORMING ORGANIZATION REPORT NUMBER
AFIT/GA/ENY/90D-12

9. SPONSORING/MONITORING AGENCY NAME(S) AND ADDRESS(ES)

10. SPONSORING/MONITORING AGENCY REPORT NUMBER

11. SUPPLEMENTARY NOTES

12a. DISTRIBUTION/AVAILABILITY STATEMENT
Approved for public release; distribution unlimited.

12b. DISTRIBUTION CODE

13. ABSTRACT (Maximum 200 words)

An investigation is conducted into low orbiting satellites around the planet Venus with drag limited lifetimes. It is possible to specify combinations of orbital elements which result in orbital lifetimes in excess of some desired value. These combinations can be assembled into Critical Curves and Critical Surfaces. Critical Curves and Surfaces are defined as curves and surfaces in orbital element space above which initial element sets will result in orbits that meet or exceed lifetime requirements.

A numerical method is implemented for finding these combinations, and three Critical Surfaces are examined. A "decay threshold" is selected for bounding satellite lifetime. Numerical simulations are conducted, and polynomials describing the Critical Curves are produced for five eccentricities at each of three decay threshold values. Comparisons are made of the effects of the different perturbations considered (geopotential, atmospheric drag, third body effects due to the sun, and solar radiation pressure).

14. SUBJECT TERMS	15. NUMBER OF PAGES
Orbital Lifetime, Low Orbits, Venus	75
	16. PRICE CODE

17. SECURITY CLASSIFICATION OF REPORT	18. SECURITY CLASSIFICATION OF THIS PAGE	19. SECURITY CLASSIFICATION OF ABSTRACT	20. LIMITATION OF ABSTRACT
UNCLASSIFIED	UNCLASSIFIED	UNCLASSIFIED	Same as Report